JET-R(96)02

High Heat Flux Exposure Tests on 10 mm Beryllium Tiles Brazed to an Actively Cooled Vapotron made from CUCRZR

H D Falter, D Ciric, D J Godden, C Ibbot, A Celentano.

JET Joint Undertaking, Abingdon, Oxfordshire, OX14 3EA, UK.

March 1996

SUMMARY

10 mm thick Beryllium tiles brazed to a CuCrZr vapotron have been shown to withstand power densities of 20 MW/m^2 for up to 2 seconds without catastrophic failure of the braze. Some of the tile surface was above liquidus temperature for up to 900 ms. A strong Be I line intensity is observed approximately 500 ms after the start of surface melting. The emissivity of the surface shows strong variations with time and location once the surface has been above liquidus. The surface damage is quite limited, however cracks are observed after several exposures above liquidus. The reflectivity for wavelengths to which the CCD camera is sensitive changes strongly once the surface has been above melting. This might cause saturation effects leading to misinterpretation. The experimental results are being used successfully by ITER and NET to benchmark numerical models.

1. INTRODUCTION

Brazing of Beryllium tiles to CuCrZr heat sinks has initially been developed at JET for a water cooled divertor [1] and tests have been carried out on 1.5, 2, and 3 mm thick tiles [2]. Later this technology was applied to 10 mm thick tiles which are more relevant for the ITER divertor and first wall components. In a first test the tiles were exposed to power densities of 5 - 6 MW/m^2 as expected for the ITER divertor [3]. The present test tries to simulate the ITER fault condition, when the radiative divertor is lost and the plasma burns through to the armour plate. The expectation is that a radiative cloud forms due to evaporation from the Beryllium armour which reduces the impinging power density and thus limits the damage to the armour tile [3]. In this test we simulate the anticipated ITER power densities to provide benchmark data for modelling. The vapour shielding itself can not be tested in this experiment as the particle energy is too high.

2. EXPERIMENTAL TEST DETAILS

The test was performed in the JET Beryllium test rig which has been previously described [2]. The test section is detailed in table 1 and is shown in Fig.1. Only the upper part of the test section with the discolouration in Fig.1 was used for the test described here. The same tiles had been exposed to 100 pulses of mostly 10s duration at power densities between 5 and 6 MW/m^2 [4]. One tile, which was used for visual examination, is removed from the test section in Fig.1.

Table 1: Test section details	
Be tiles	27 x 27 x 10 mm^3, uncastellated, Beryllium grade S65C
braze cycle	induction braze at 720°C with InCuSil "ABA" braze
heat sink	27 mm wide vapotron with 4 mm fin height and 3 mm fin width and fin spacing and 8 mm high water channel.
water flow rate	4.3 m^3/h - corresponds to 7.7 m/s
water inlet temperature	20°C
water pressure	approximately 6 bar in the test section
water pressure drop	4.4 bar

2.1 Test geometry

The test section was installed vertically behind a scraper with the outer 4 mm of the test section shielded by one of the scrapers. A copper calorimeter with 16 mm spacing between the individual calorimeters was installed beside the test section and used for measuring the vertical profile and the power density. Both test section and copper calorimeter are inclined by 80° against the beam normal. A schematic plan view of the experimental set-up is shown in Fig2.

2.2 Diagnostics

The surface of the test section is viewed by an IR imaging system and by a video camera. The IR system can either run in frame mode with a repetition rate of 30 Hz or in line mode with a repetition rate of up to 2.5 kHz. Most of the measurements were done in line mode. The highest calibrated range is 500 - 2000°C which allows measurements above 2000°C for emissivities <1. In this high temperature range a narrow bandwidth filter is used with maximum transmission at 2.8 micron. The viewing angles are shown in Fig.3 which gives the elevation view of the test rig. Power density is measured with both an inertial copper calorimeter and water calorimetry. In the case of water calorimetry we measure the absorbed total energy E_{tot} and get the peak power density p_{max} via

$$E_{tot} = p_{max} \times w \times \tau \times \int p(z)/p_0 dz$$

with w = exposed width of the test section, τ= exposure time, and $p(z)/p_0$ as normalised vertical power density.

It should be noted that both measurements give a power density averaged over the width of the test section.

2.3 Power density profile

The vertical profile can be derived from the inertial calorimeter. Fig.4 gives an example for a pulse with steady state conditions (6s) and modest power densities (7.6 MW/m^2). On the vertical profile the peak power density extends over approximately 80 mm which corresponds to the width of 3 tiles.

On the horizontal profile the temperature drops by approximately 20% over the width of the tile. The peak power density extends over roughly 5 mm.

The power density from water calorimetry and from the inertial calorimeter agree generally quite well (Fig.5) with a scatter of ±10% if plotted against extracted power. In the case of modulated beams, which were used for the pulses with melting, the scatter of the water calorimetry is larger.

2.4 Beam properties.

The tiles were exposed to a hydrogen beam with an energy of typically 75 keV/amu in the full energy component. The beam is approximately 40% neutralised with roughly 70% of the power in full energy particles, the rest in particles of 1/2 and 1/3 of the full energy . The pressure in the vacuum chamber during exposure is approximately 4 µbar of hydrogen.

2.5 Beam modulation.

The power density in the beam was constant during a pulse. The average power density on the test section can be varied by modulating the beam (on/off modulation). The modulation sequence used throughout this test was:

1. Modulation with 18 ms on every 80 ms for 4 seconds (average power density is 22.5% of the peak power density) followed by

2. beam full on for up to 1.5 seconds followed by

3. modulation with 12 ms on every 34 ms (average power density is 35% of the peak power density) for approximately 2 seconds.

The error in measuring the on time is approximately 1 - 2 ms per reapplication, which can influence the actual average power density by up to 20% in the case of the modulation sequence 3. Additionally the power density in the modulated phase can be reduced by natural breakdowns which increase the off time and reduce the on time. A typical current trace is shown in Fig.6.

3. TEST SEQUENCE

The test was carried out in several steps with visual examinations of the tile between each step. The sequence was as follows:

1. Exposure to long pulses with surface temperatures up to 1000°C.

2. Exposure to modulated beam with a peak power density of 20 MW/m^2 and the power density profile described above in 2.5 (22.5% - 100% - 35%). 1s of permanent beam on and with part of the surface above liquidus for up to 300 ms.

3. Same modulation as in 2 but with 1.3 s permanent beam on and with some of the surface above liquidus for up to 700 ms in 2 pulses.

4. Same modulation as in 2 but with 1.5 s permanent on (800 - 900 ms above liquidus for 4 pulses).

5. Calibration of the IR imaging system.

The calibration of the IR imaging system was done after the experiment and will be explained later. For all the measurements we used an emissivity of 0.35 which had been measured previously on several experiments with Be S65C. Some measurements were then reprocessed using the emissivity as measured at the end of the experiment.

4. EXPERIMENTAL RESULTS

The experimental results are listed here in sequential order starting with unmodulated beams and surface temperatures up to 1000°C, followed by the melt experiment, and finally the calibration of the surface temperature measurement.

4.1 Pulses without melting.

This part of the experiment was performed to establish that the tiles could be heated up to surface melting without being damaged. The beam ontime was increased in steps at fixed power density until the surface temperature approached 1000°C. After that the pulse sequence was repeated with a higher power density. The power density was increased in steps from 7 to 14 MW/m^2. The surface temperature rise followed an exponential law with a time constant of 2.9s. The surface temperature as a function of time and the curves fitted to the data are shown in Fig.7. In the case of equilibrium the surface temperature can easily be calculated with a one dimensional model using a projected heat transfer coefficient of 70 000 W/m^2/K between vapotron and water [5] and the temperature dependent thermal conductivity of Beryllium [6]. As

Fig.8 shows, the agreement is acceptable. The fits in Fig.7 are done below 1000°C where the thermal conductivity of Beryllium is well known. The good agreement suggests that the measurements of surface temperature and power density are both correct, as simultaneous wrong measurements in which the errors cancel are unlikely. This means that the IR imaging system gave reasonable results at this stage with the usual emissivity of 0.35. It will be shown below that the measured surface temperatures were far too high after the first surface melting had occurred.

The main result from the test was, that the tiles are strong enough for the melting experiment. Initially all tiles had a good uniform thermal contact to the heat sink as can be seen from the uniform temperature distribution in Fig.9.

Exposure time and power density of this test sequence is shown in Fig.10. The pulse parameters are listed in Annex 1.

4.2 Pulses with surface melting

The pulse statistics are shown in Fig.11 and Annex 2 for all three parts of the test.

4.2.1 Exposure with up to 1s at 20 MW/m^2

The first sequence was terminated after the pulse in which the unmodulated beam on time reached 1 second. Using an emissivity on 0.35 the surface temperature from the IR imaging system reached 2000°C, but there was no visual sign of melting on the display of the video system. Visual examination of the test section did not show any signs of melting (Fig.12a). There was however a clear change in colour from blackish to grey in the area which was above the liquidus temperature. A closer examination of the temperature / time dependence showed that the cooldown is delayed, which must be caused by resolidification of molten material. This is shown in Fig.13 in an expanded view. At the same temperature we also see a change in slope during the temperature rise phase. This observation gives a calibration point for the IR imaging system and we can determine the length of time for which the temperature was above liquidus (Fig.11). Temperature profiles along one tile, taken every 2 ms, show that the tile centre cools down before the edges, which means that in this case the melting was deeper at the edges (Fig.14).

4.2.2 Exposure with up to 1.3 s at 20 MW/m^2.

In this run the exposure at full power density was increased to 1.3 seconds and the time above melting was up to 0.7 seconds for 2 pulses. Fig.15 shows the surface temperature of the hottest spot as a function of time. In the case of Fig.15 the surface temperature is corrected with the emissivity from the IR calibration. The onset of melting and the resolidification is clearly visible. Also plotted in Fig.15 is the intensity of a BE I line. This line intensity has the same

temperature dependence as the evaporation rate from literature [6]. In the case of Fig.15 it appears that the surface temperature saturates just above 1400°C as could be expected from the additional energy loss mainly due to melting, radiation, and evaporation. However this observation could not be repeated in successive pulse - probably because of the strong variation in surface emission with temperature and time which will be dealt with later.

The tile surface after the second cycle shows a significant discolouration pattern: black near the scraper were the power density is lower, followed by a grey and a darker ring which encloses a grey area (Fig.12b). The hottest area shows already some cracks and is also darker. Another interesting observation from this view is that the copper scrapers are black - most probably covered with sputtered Beryllium. The scrapers are at an angle of 30° against the beam normal and erosion appears to be smaller than deposition.

4.2.3 Exposure with up to 1.5 s at 20 MW/m^2.

In this series we had problems with the IR imaging system which stopped recording during the first three pulses, probably due to noise from breakdowns. The first fully recorded pulse was done after three unsuccessful attempts. The output of the IR imaging system is now quite confusing with local hot spots and with hotter areas appearing and disappearing during the pulse - probably a consequence of the damage of the tiles near the surface from previous pulses. This is demonstrated in Fig.16 with the time development of the vertical temperature profile along 4 tiles. At the left side a temperature maximum builds up (a), the hot spot (b) remains essentially unchanged and the peak (c) disappears during heat up. The onset of melting and the resolidification are now obscured. The increased radiation from the damaged surface is however not catastrophic with typically 400°C excessive temperature at 20 MW/m^2. The extend of the tile damage after four pulses with part of surface above liquidus temperature for 800 - 900 ms is shown in Fig.12c. The tile surface shows cracks, holes, and white lines. The melting is up to 0.7 mm deep and there is a clear undercut at the braze interface (Fig.17a). Some of the molten material has disappeared, especially at the edge (Fig.17b).

4.3 Tile integrity.

4.3.1 Thermal tile response.

To assess changes in tile integrity, we repeated long unmodulated pulses with modest power density of approximately 5 MW/m^2 after each of the above exposure sequences. Contour plots of these pulses are shown in Fig.18. Initially the surface temperature distribution is quite uniform. After the first sequence with melting one tile is hotter than both neighbours. After the second sequence with surface melting the two middle tiles are hotter than the outer neighbours and we see the grey line in Fig.12b as a region with increased gradients. Finally after the third melting sequence we have some hot spots with a temperature excess of up to 300°C compared

to that of the neighbouring area (Fig.19). This might still be acceptable for operation at 5MW/m^2.

A puzzling observation is that the surface appears quite differently depending on what is used to view it. Fig.20 shows a video picture taken from the same location and after the same tile exposure as Fig.12b. The video picture was taken by illuminating the tile inside the test rig with a fibre from outside and the right side of the beryllium tiles appears white, indicating a large reflection of light. The method is similar to that used for in vessel inspection systems and can be misleading, if the camera goes into saturation due to excessive exposure. One would get an impression as if the surface is distorted due to melting.

4.3.2 Micrographic examination of the hottest tile

The top layer of the hottest tile has been cut off by spark erosion for visual examination after the test. The molten area can be clearly identified by a completely different grain structure Fig.21. The maximum melt depth is 0.7 mm. Cracks through the molten area partially penetrate into the base with a depth of approximately 0.5 mm but there are also cracks confined to the melt layer and cracks in areas without melting. Occasionally part of the molten material has disappeared. There is no evidence of lateral cracks and the melt layer appears to be solidly attached to the base material.

4.3.3 Ultrasonic test of the braze connection after the test

The undercut between beryllium armour and CuCrZr heat sink shows up as a distortion of the contact in an ultrasonic test carried out after the exposure sequence. All heavily exposed tiles show reduced contact at the side with the highest power density (bottom in Fig.22) and the two adjacent sides. The tiles are still well contacted in a roughly circular area with approximately 20 mm diameter. The centre of this well contacted area is shifted towards the side with the lowest power density (top in Fig.22) and the edges at the side with the highest power density shows the largest braze damage. The local faults on the ultrasonic are likely to be caused by melt damage at the surface rather than localised damage at the braze.

4.4 Calibration of the IR system.

For the calibration of the IR imaging system the whole test section was heated up without cooling. When the temperature had equilibrated we compare the output of the IR system with thermocouple measurements and adjust the emissivity to match both temperatures. In this test the emission from the surface was very **non** uniform (Fig.23) and we have to use a complicated emissivity profile to reproduce a constant surface temperature. To derive the temperature dependence of the emissivity we use the following calibration procedure: The transfer function of the IR system is

$$T = \frac{B}{\ln(\varepsilon\tau R/I + F)} \tag{1}$$

B, R, and F are calibration constants set by the manufacturer. ε and τ are emissivity and transmission and I is the intensity of the source signal. The direct output of the imaging system is the temperature T. With the intensity I fixed we can calculate the emissivity we need to match surface and thermocouple temperature in (1). The calibration was done in the range 100 - 500°C and the result is presented in Fig.24. Being mainly interested in areas with melting, we can get an additional data point at the onset of melting, which is at 1289°C. To get the emissivity of the solid material the data point from melting is slightly lifted up to 1330°C to compensate the temperature rise observed with the onset of melting. This gives us an emissivity fit for the area with surface melting:

$$\varepsilon = 0.63 - 0.55 \times e^{T/140°C} \tag{2}$$

(2) is used before the onset of melting. It appears that the emissivity is essentially constant above 500°C. Above melting we use a constant emissivity of 0.68, which is derived from the transition temperature.

With the emissivity in (2) the calibrated surface temperature T_C is then:

$$T_c = B \Big/ \left\{ \ln\left(\frac{\varepsilon}{\varepsilon_0} \left(e^{B/T_0} - F \right) \right) + F \right\} \tag{3}$$

B and F are the calibration constants in the respective temperature range, T_0 is the temperature measured with the emissivity ε_0 set at 0.35 throughout this experiment.

The high emissivities observed in this experiment were surprising to us. In previous experiments we measured emissivities of 0.15 - 0.2 on the material before exposure. With exposure to energetic hydrogen beams the surface blackened and the emissivity increased to 0.35.

Higher emissivities are reported from Beryllium Oxide [7] but it is not obvious, why this oxide should be formed more vigorously when the surface is close or above the liquidus temperature.

5. DISCUSSION

5.1 Emissivity

The pronounced temperature dependence of the emissivity as observed after the melting was not expected and not observed in our previous experiments. It appears that the temperature

dependence is a consequence of the melting. This can be concluded from the good agreement of measured and calculated temperature in Fig.8.

5.2 Depth of the melt layer.

In Fig.15 we see a delay in cooldown due to resolidification by 100 ms. From Fig.8 we can deduce that the equilibrium heat removal rate of the target cooling is approximately 8.7 MW/m^2 when the surface temperature is at the liquidus temperature of 1289°C and we conclude that 8.7MW/m^2 is released in the resolidification. With a heat of fusion of 1132 J/gr this means that 77 mgr have to fuse to explain the delay in cooldown. This corresponds to an average melt depth of 0.42 mm. In the case of Fig.15 the surface was above melting for 700 ms. In the pulses with the longest exposure the surface was 900 ms above the liquidus temperature and the average melt depth is estimated at 0.53 mm. This compares with up to 0.7 mm melt depth seen in Fig.21.

5.3 Vapour shielding

The Beryllium line intensity in Fig.15 is very similar to that of a neighbouring Balmer line from the hydrogen background. From that we can assume that beam attenuation from the hydrogen is larger than that from the Beryllium vapour shield as the path length in hydrogen is 2 m while that in Beryllium is probably of the order of the tile width. For lower particle energies the result would be different. In this experiment we can not expect to see the effect of vapour shielding in form of a reduction in the impinging power density and thus the result is not relevant to the case of plasma impinging to a divertor. The variation of the line intensity with surface temperature indicates, that we observe the sublimation as expected from literature. Using simple gas kinetics we can correlate the vapour pressure to an evaporation rate de/dt

$$\frac{d}{dt}e = \frac{p}{6m}\sqrt{\rho_0/p_0}$$

where p is the vapour pressure, m is the mass of the evaporated material and ρ_0 is the density at the pressure p_0. For Beryllium this gives us an evaporation rate

$$\frac{d}{dt}e = 5.5 \times p\left[\frac{mbl}{s\ cm^2\ Torr}\right].$$

For the highest temperature in Fig.15 this gives an evaporation rate of approximately 2 $mbl/s/cm^2$.

In the case of first wall applications the formation of charged clusters, which might form from the liquid in the field of a plasma sheath, could be an additional mechanism for increased erosion.

5.4 Comparison with model calculations

Model calculations of actively cooled Beryllium targets above liquidus temperature have been developed by the ITER JCT [8,9,10] and the European ITER home team [11].

In the case of the ITER model "RACLETTE" two iterations were used with 20.5 and 19.5 MW/m^2 during the unmodulated phase and 8 and 6.5 MW/m^2 during the final modulation. The result is shown in Fig.25. With the nominal power density of 20.5 MW/m^2 during beam on, 4.5 MW/m^2 for the preheat phase and 8 MW/m^2 after the melt phase the calculated temperature is approximately 80°C above the measured temperature during the heat up. The time of the first melting is correct in the model, the time for resolidification however is too long. Reducing the power densities to 19.5 MW/m^2 for the heat up phase and 6.5 MW/m^2 for the final phase gives a good match for the initial temperature rise and the time for resolidification is also correct. The time of the first melting is however delayed by 300 ms with respect to the experiment. This indicates that a peak power density of 20 MW/m^2 is probably correct. After the melting a power density of 6.5 MW/m^2 gives reasonable agreement. Also shown is the net heat flux through the Beryllium calculated with 19.5 MW/m^2 of incident flux. With the onset of melting the net heat flux is gradually reduced to 14 MW/m^2.

The 2d finite element model from NET shows quite similar results (Fig.26). In this calculation the power density in each of the three phases has been adjusted individually to optimise the agreement with the measurement. The power densities used are well within the experimental error of the measurement.

In comparing both results one should keep in mind that the temperature measured is not too accurate because of the varying emissivity and the calculations use extrapolated material data above 1000°C. Additionally in the NET 2D model a lower power density is used for the final modulation to improve agreement.

5.5 Braze integrity

There is a clear tendency for the edges of the Beryllium to pull away from the heat sink. With the limited number of pulses the failure was not catastrophic and the tiles were still reasonably well cooled. For the application in a divertor a design with reduced stress has to be developed.

5.6 Relevance to Fusion experiments:

Although we can not simulate the vapour shielding process itself we can draw some conclusions which are relevant for a Divertor:

- **At 20 MW/m^2 the vapour emission becomes significant when the melt layer is approximately 0.5 mm deep. This shallow melt layer appears to have a reasonable**

strength and can sustain several exposures without catastrophic damage. The evaporation is as expected from literature.

- **If the power density is lower the melt layer will be deeper before vapour emission becomes significant. A deeper melt layer is expected to have less strength and will be lost faster. A thicker armour is therefore expected to have a larger erosion rate.**

- **In case of power densities just large enough to cause surface melting, the melted layer might become unstable before the evaporation rate is large enough to reduce the incipient heat flux.**

- **Periodic structures on the surface of metals after melting have been reported [12] from metals with impurities. These structures are not apparent on our surface (Fig.12c and 18).**

REFERENCES

[1] C Ibbot et al, "Further developments of brazing Beryllium to CuCrZr"2. Proceedings of the 18th Symposium on Fusion Technology (SOFT 18) held in Karlsruhe 22-26 August 1994 also in JET-P(94)40 pp 175 - 180

[2] H D Falter et al, "Testing of plasma facing materials for divertors in the JET Neutral Beam Test Bed", SPIE Vol. 1997 High Heat Flux Engineering II (1993) 170 - 181.

[3] G Janeschitz, A Antipenkov, S Chiocchio, J Dietz, G Federici et al,"The physics basis and design of the ITER divertor and of the pumping, fuelling system, IAEA-CN-60/E-P-6, Seville, Spain, Oct 1994

[4] H D Falter, D Ciric, "10 mm thick Beryllium tiles brazed to a CuCrZr vapotron - Test Report", Internal Report JET-C(94)128

[5] H D Falter at al, "Thermal test results of the JET divertor plates", SPIE Vol. 1739 High Heat Flux Engineering (1992) 161 - 172. H D Falter, E Thompson, "Performance of Hypervapotron Beam Stopping Elements in JET", JET-P(95)13 - submitted for publication to Fusion Technology.

[6] D E Dombrowski, E B Deksnis, M A Pick, "Thermomechanical properties of Beryllium", JET-IR(94)07

[7] R L Seifert, "The spectral emissivity and total emissivity of Beryllium Oxide", physical review, vol 73, No 10, pp1181 - 87, May 1948

[8] G. Federici, A. R. Raffray et al., "Analysis of heat transfer and erosion effects on iter divertor pfc's induced by slow high-power transients", to be presented at the 16th IEEE/ NPSS, Symposium on Fusion Engineering, Champaign, IL, Sept. 30/Oct. 5, 1995.

[9] A. R. Raffray and G. Federici, Raclette: "A model for evaluating PFC thermal response during slow-high, power transients - Part I: Theory and Description of Model Capabilities", to be submitted to J. Nucl. Mater.

[10] G. Federici. A.R. Raffray and B. Esser, Raclette: "A model for evaluating PFC thermal response during slow-high, power transients - Part II: Analysis of ITER Divertor and First Wall PFCs", , to be submitted to J. Nucl. Mater.

[11] I Smid et. al. "2D finite element analysis of plasma excursions at 29 MW/m^2 , including vapour shielding, onto Be-, CFC-, and W5 Re-armoured ITER divertor plates", NET Internal Report N/I/3330/16/A

[12] V V Vladimirov, M D Gabovich, I A Solochenko, V A Khomich, and V VTsiolko, "Impurity mechanism for the excitation of short wavelength periodic structures on the surfaces of a solidifying melt", Sov. Phys. JETP 73 (3) p 465 (Sept 1991).

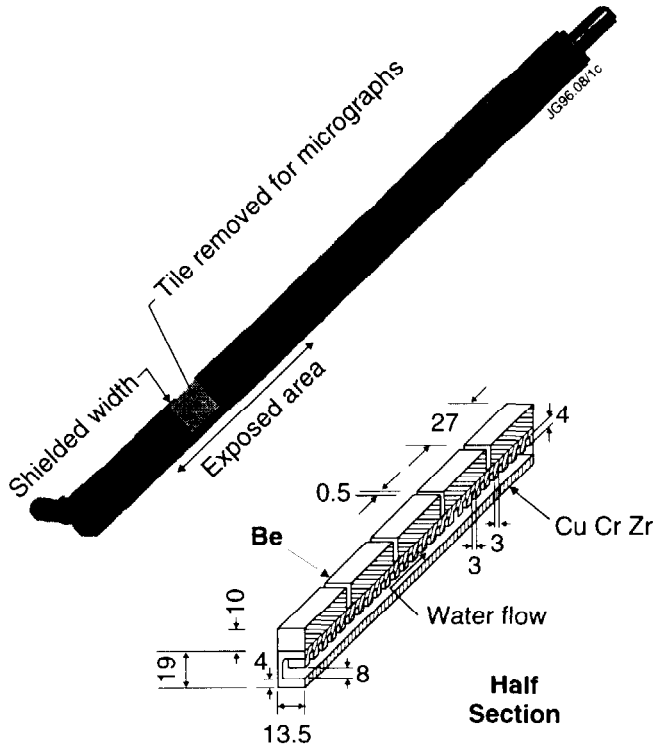

Fig. 1: Photograph of the test section after the test (top) and schematic cross section.

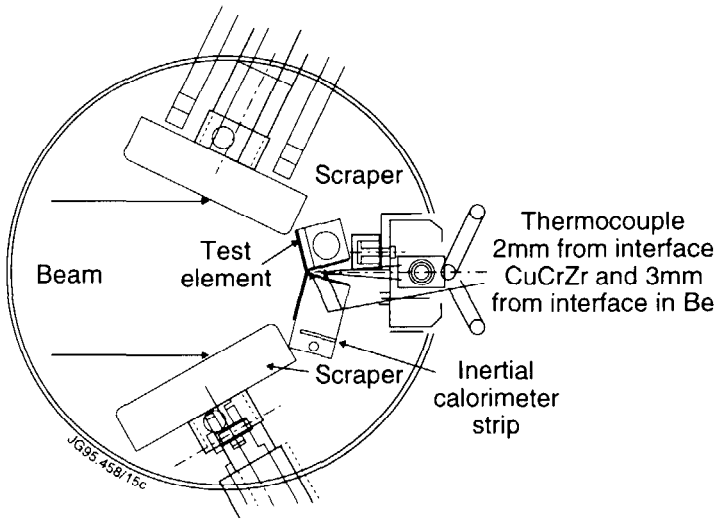

Fig. 2: Plan view of the test setup. The test section is installed behind vertical scrapers with a copper calorimeter array right next to the test section.

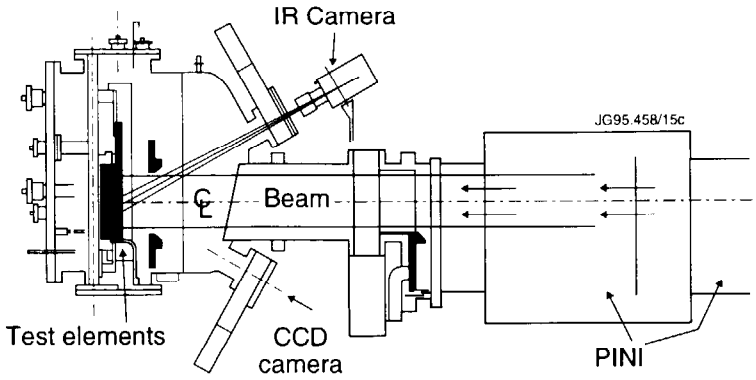

Fig. 3: Elevation view of the beryllium test rig. The test section is viewed by the IR imaging system and by a S-VHS CCD camera under an angle of 30^0. The viewing field is limited top and bottom by scrapers.

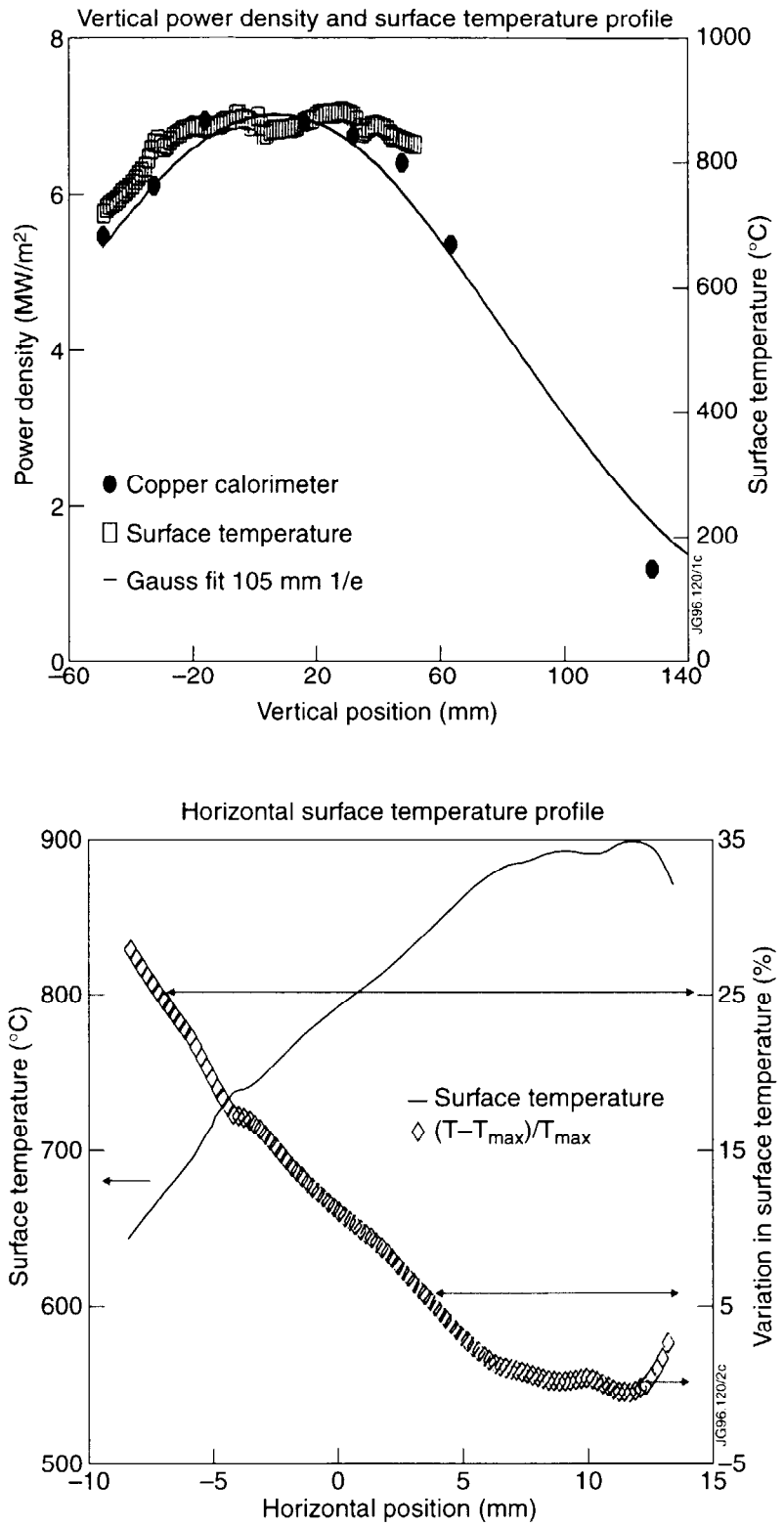

Fig. 4: Vertical and horizontal power density and temperature profiles on the test section. The power density is almost constant in the vertical plane for ±40mm from the centre line. In the horizontal plane the temperature falls by 20% over the test section with first 5mm from the middle corner at constant temperature.

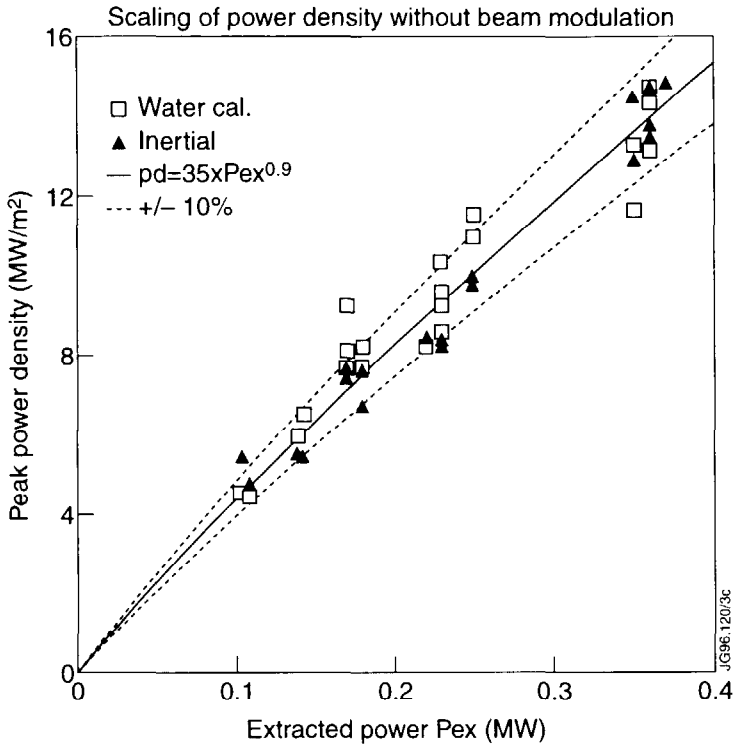

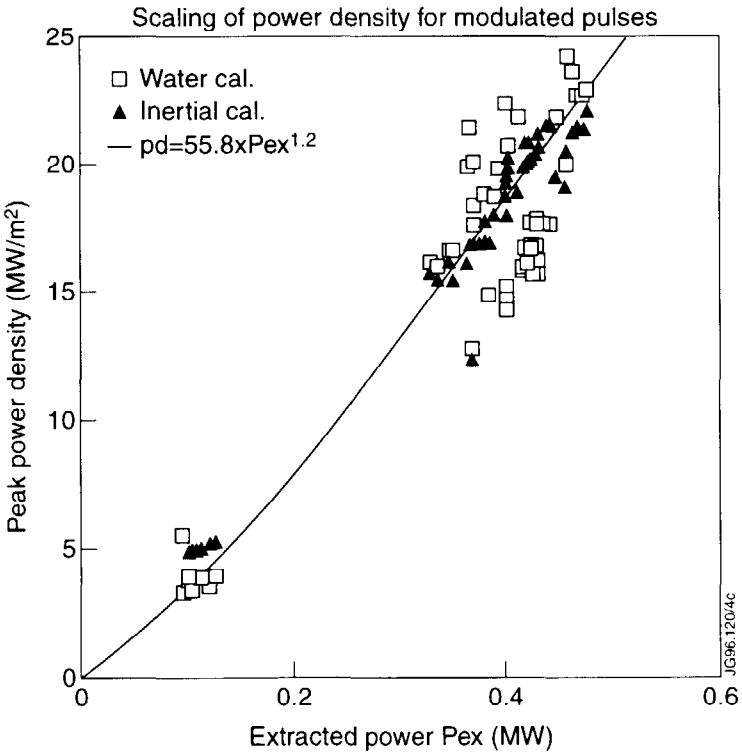

Fig. 5: Power density. The agreement between water calorimetry and inertial calorimetry is within ±10% for unmodulated beams. With modulated beams the scatter in water calorimetry is larger. The inertial data are well represented by a power law of the extracted power.

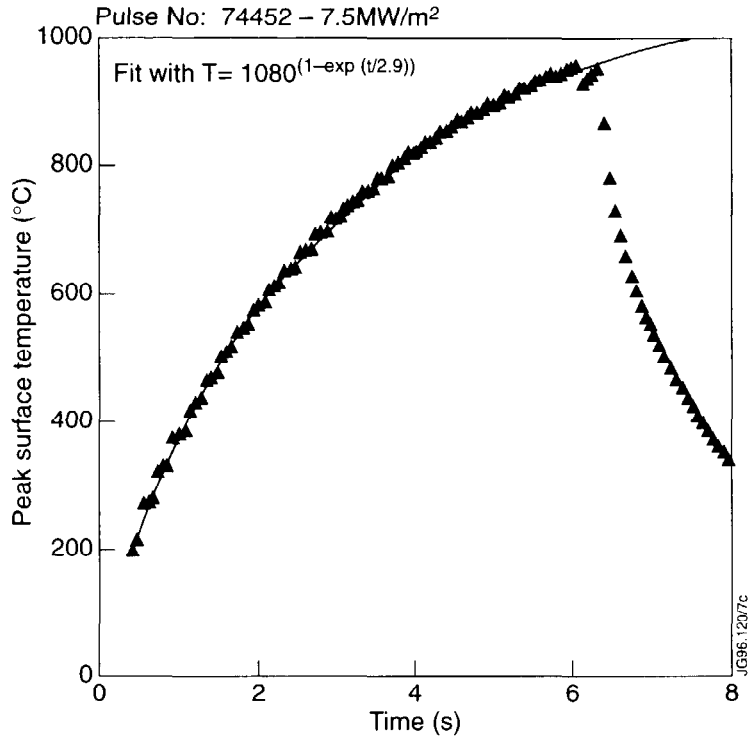
Pulse No: 74452 – 7.5MW/m²
Fit with T= 1080(1–exp (t/2.9))
Peak surface temperature (°C)
Time (s)
JG96.120/7c

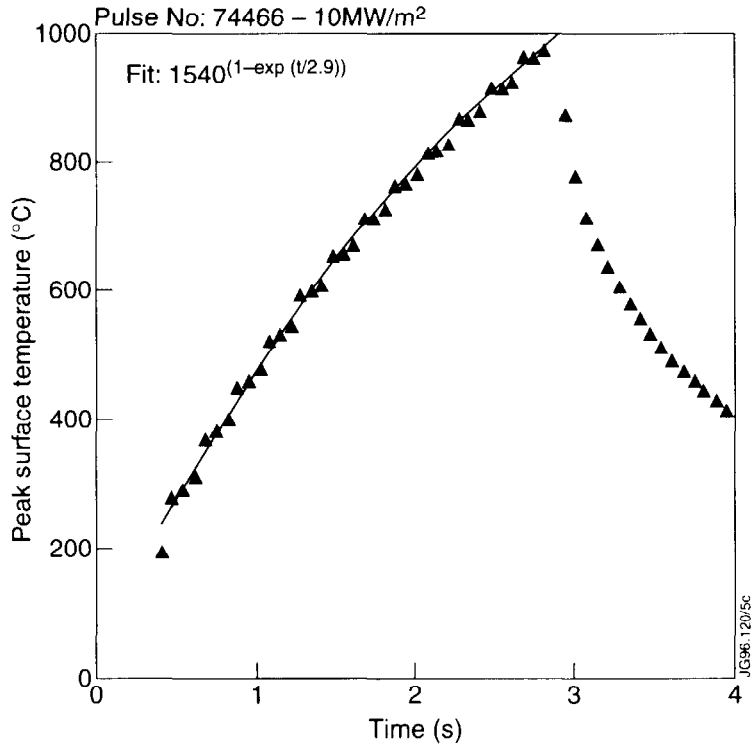
Pulse No: 74466 – 10MW/m²
Fit: 1540(1–exp (t/2.9))
Peak surface temperature (°C)
Time (s)
JG96.120/5c

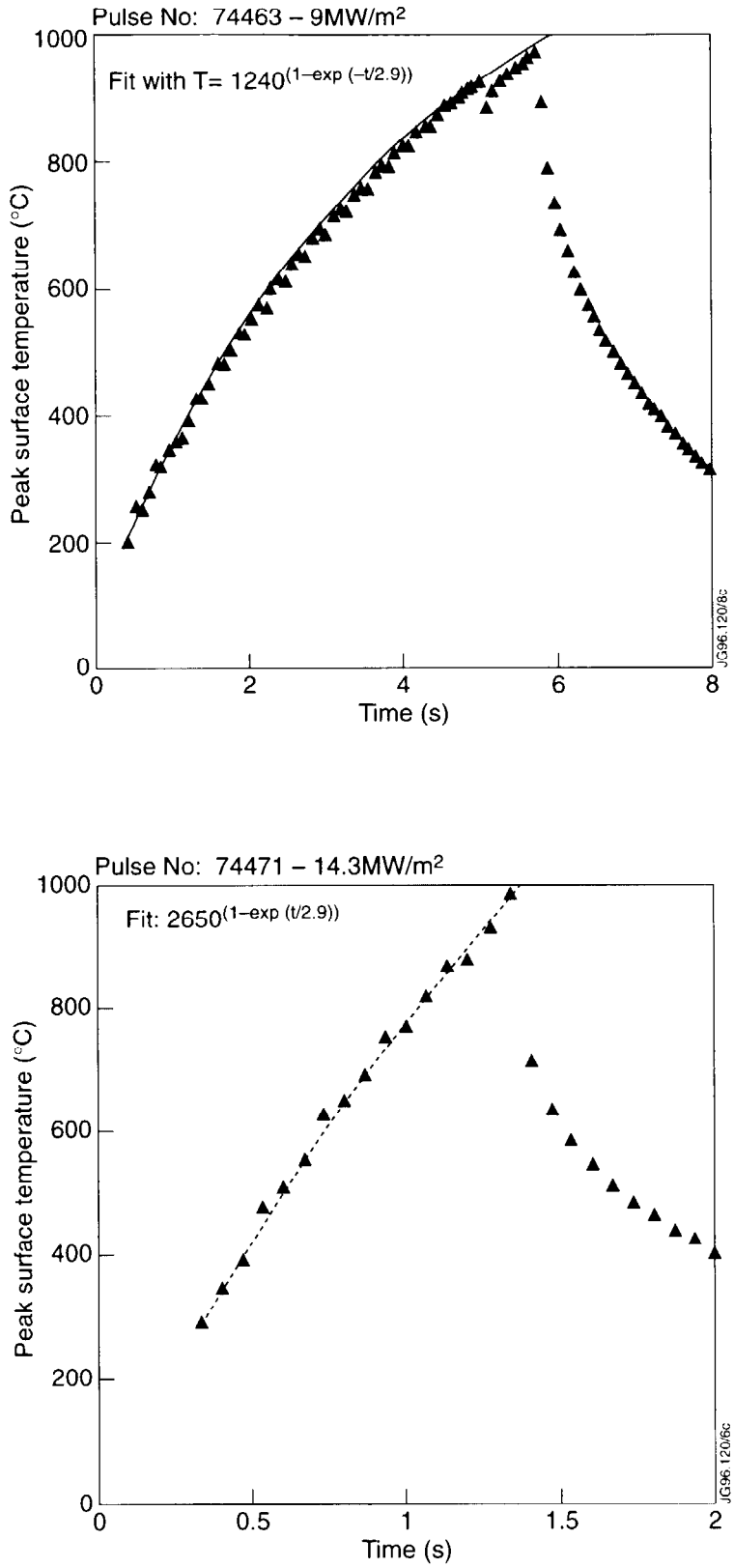

Fig. 7: Surface temperature rise for unmodulated pulses. The experimental fits give a time constant of 2.9 s and allow to extrapolate to an equilibrium temperature.

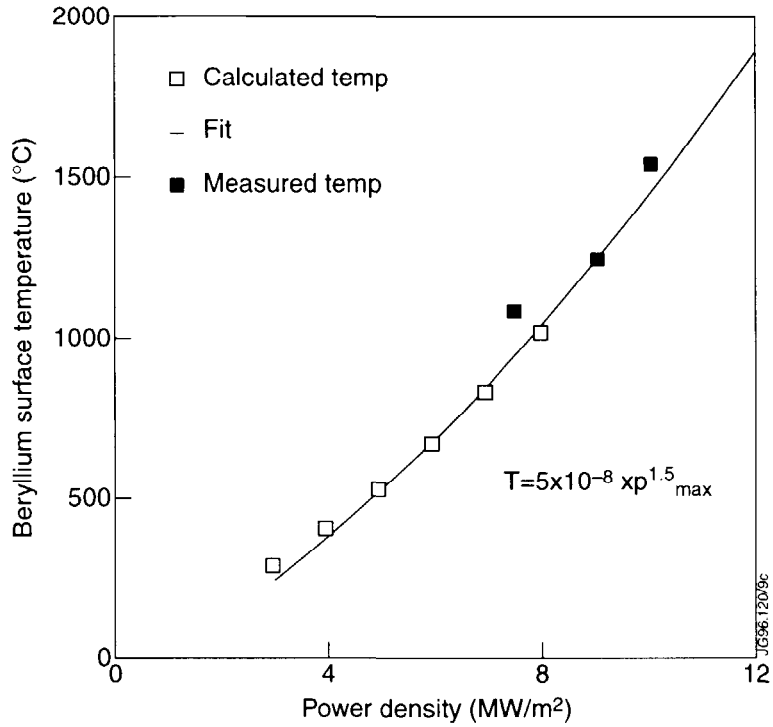

Fig. 8: Comparison of measured and calculated temperatures. Temperatures were calculated using steady state conditions, the temperature dependent conductivity of Beryllium (extrapolated data above 1000 ^{0}C) and a fixed heat transfer coefficient into the water. The equilibrium temperatures from Fig. 7 are lying on the curve that fits the calculated temperatures.

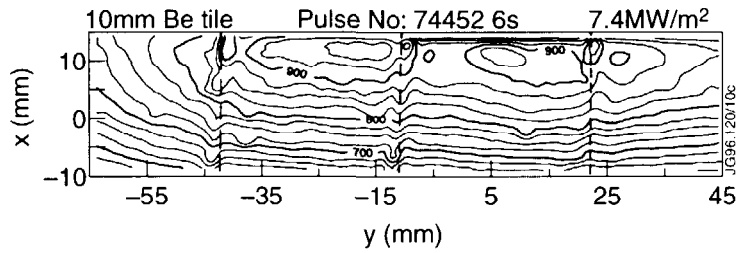

Fig. 9: Surface temperature distribution at the end of a 6s pulse. The temperature distribution over 4 tiles is uniform.

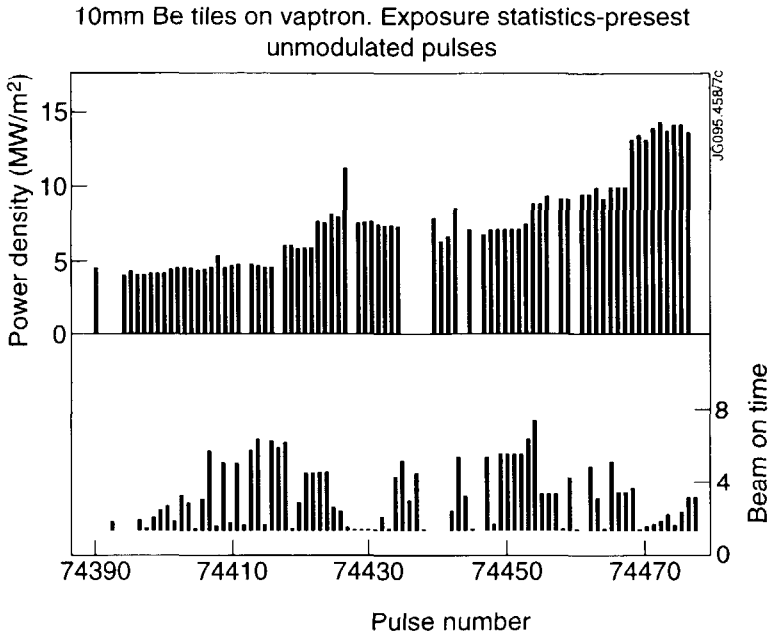

Fig. 10: Exposure statistics for the pre-test with unmodulated beams. Beam on times (bottom) are up to 5 s, power densities (top) up to 15 MW/m^2.

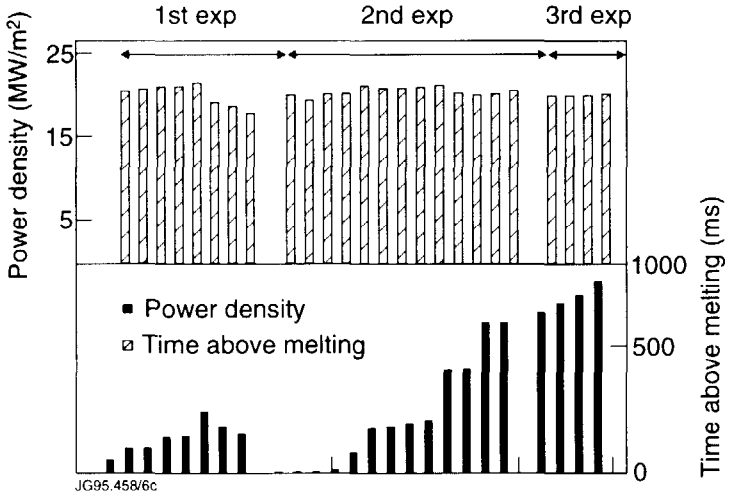

Fig. 11: Exposure statistics for the test with modulated beams and surface melting. The power density is roughly 20 MW/m^2 during beam on. The time at which the hottest area was above liquidus (shown on the right scale) was 300 ms in the first part, 700 ms in the second part, and 900 ms in the final part.

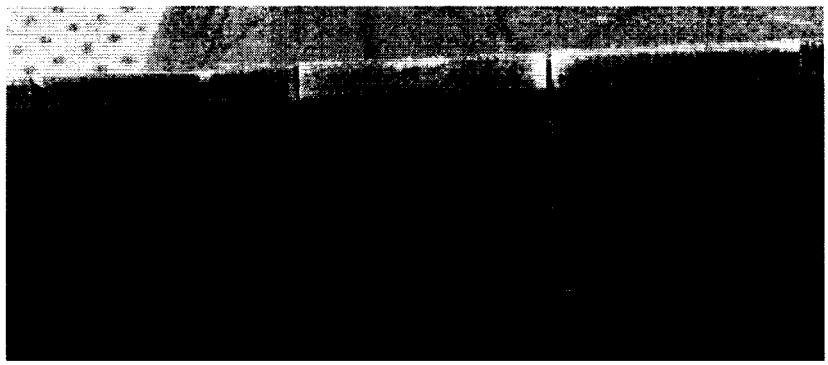

Fig. 12a: Beryllium surface after the first series with surface melting for up to 300 ms. The surface shows discoloration but no distortion. The grey colour probably marks the area which was above liquidus.

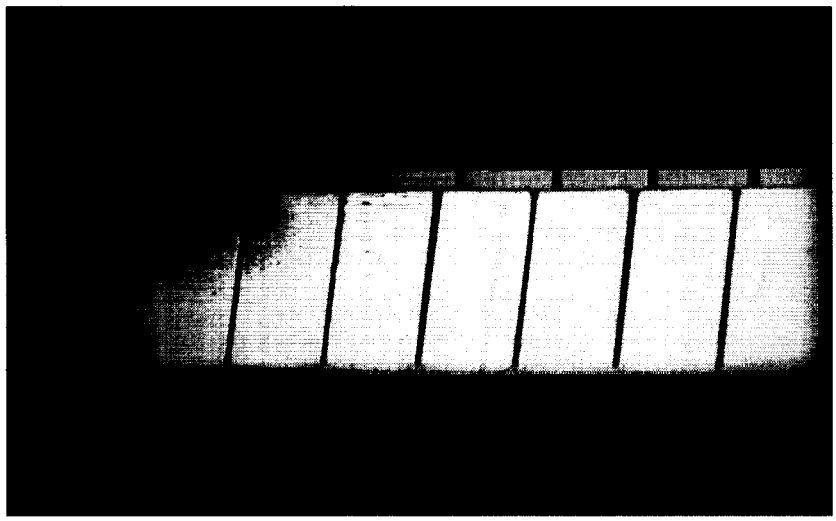

Fig. 12b: Beryllium surface after the second series with melting for up to 700 ms. The picture is taken through the window of the IR viewing system. The grey area is enlarged and the surface shows small cracks and holes on two tiles.

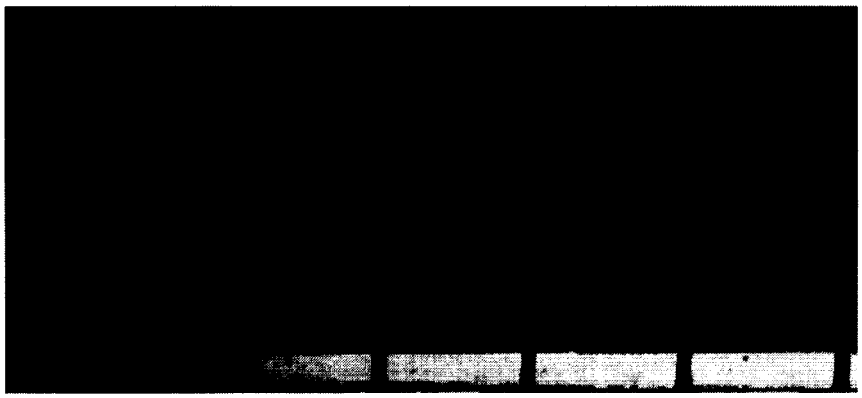

Fig. 12c: Beryllium surface after the third series with surface melting up to 900 ms. The surface shows cracks, holes and white lines. The grey area has become blacker.

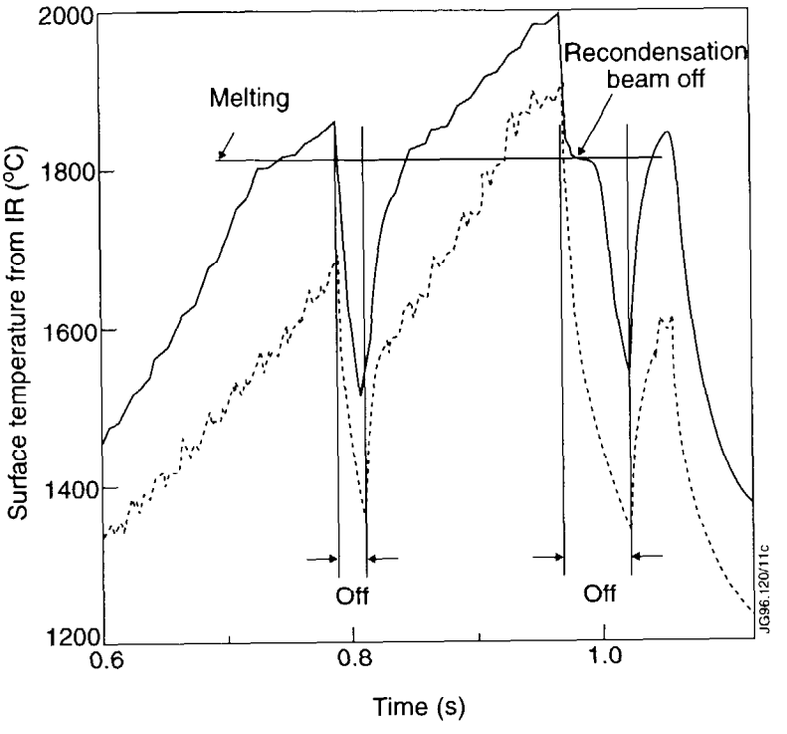

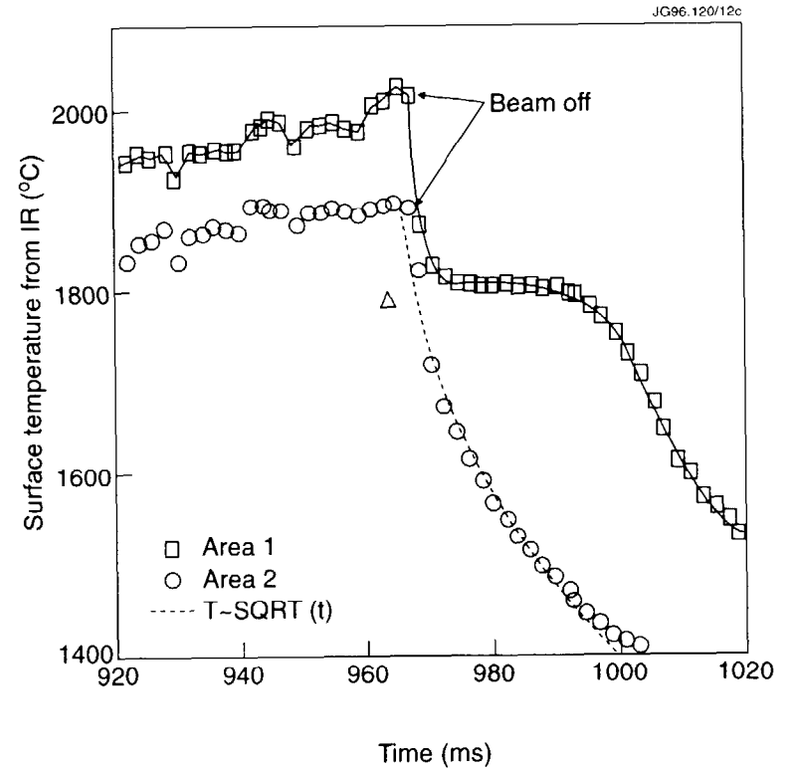

Fig. 13: Melting and recondensation. The top curve is taken from the hottest area, the lower curve is taken 10 mm away from the hottest area. Melting and recondensation are clearly visible. When the beam is turned off the temperature decays with a credible time constant confirming that the radiation is from the bulk surface.

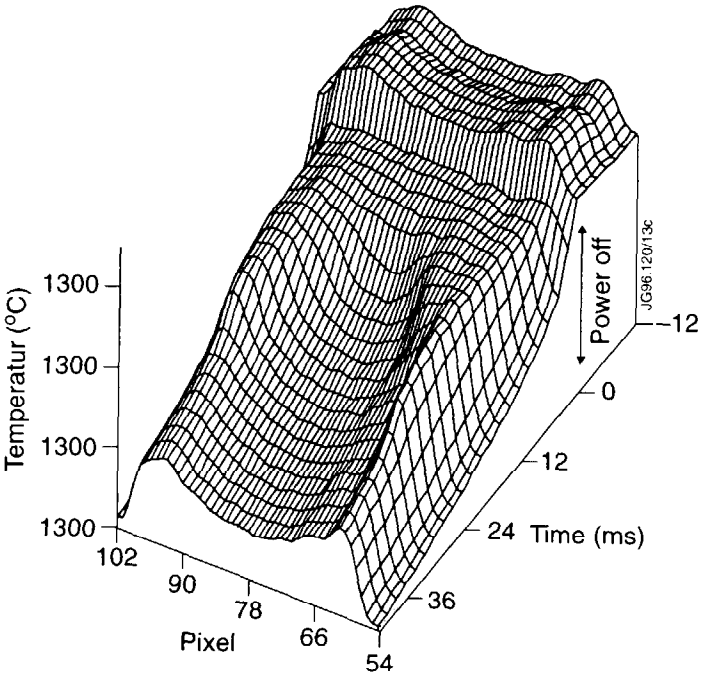

Fig. 14: Cooldown of one tile with surface melting. While the surface is liquid, the temperature is uniform across the tile. Cooldown at the edges is delayed indicating a deeper melt layer.

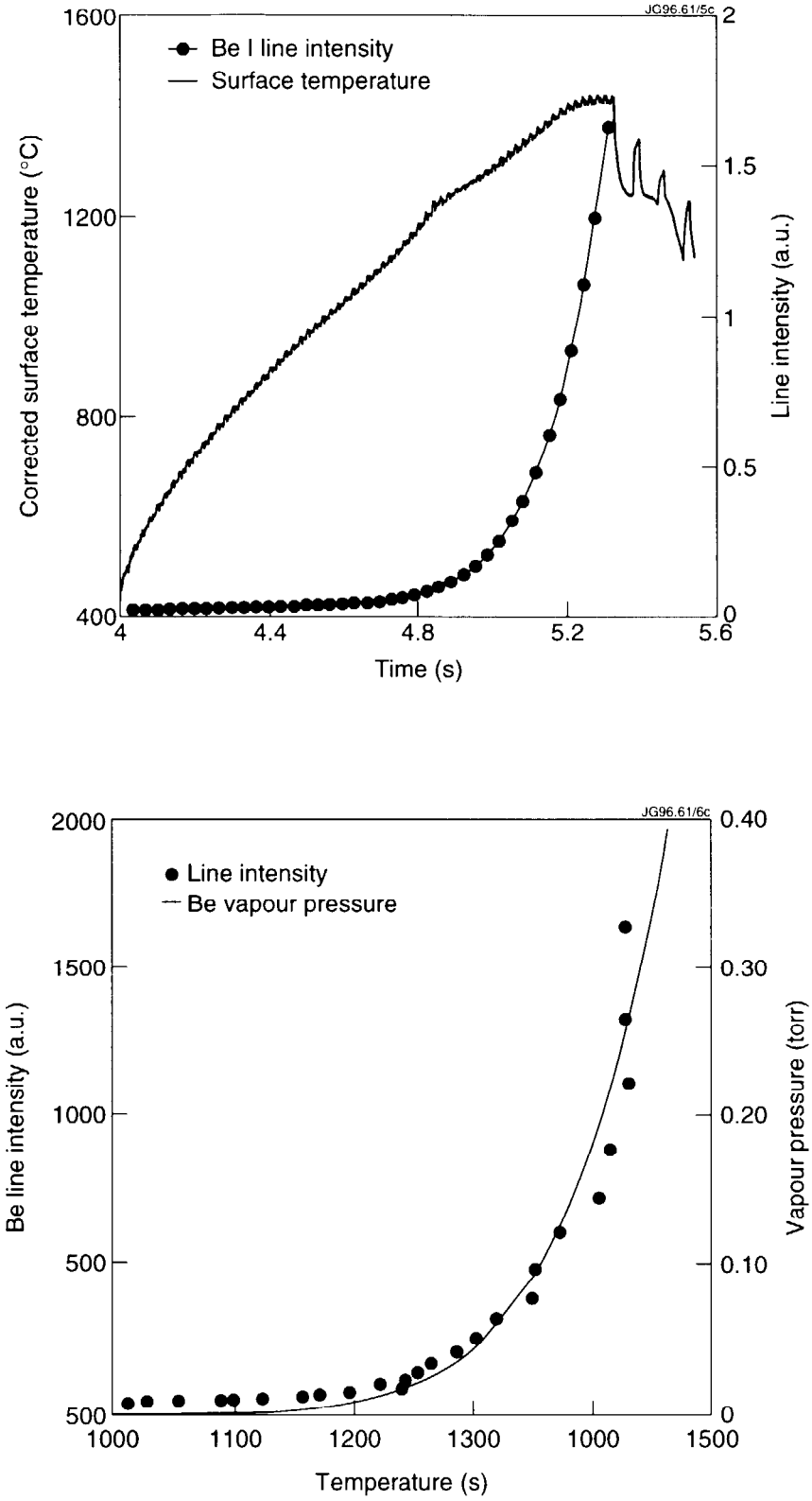

Fig. 15: Corrected surface temperature and intensity of a Be I line for a pulse at the end of the second series (700 ms of surface melting). The temperature is corrected with the emissivity from the calibration (Fig. 24).

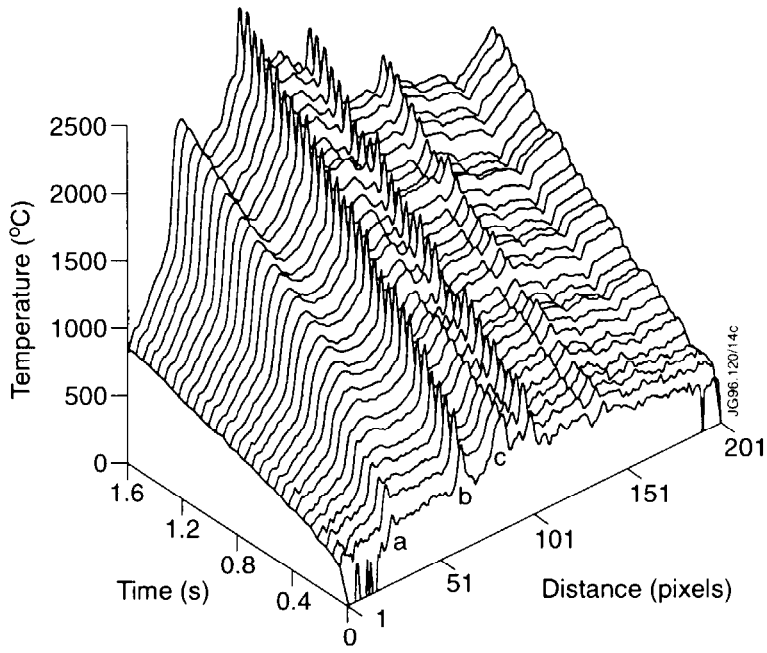

Fig. 16: Surface temperature as measured at the end of the third sequence with surface melting up to 900 ms. Due to the melt damage the radiation from the surface becomes erratic: Maxima form (a) and disappear (c). Some spikes persist (b). Nevertheless the overheating is ***not*** *catastrophic in the sense that most of the incident power is radiated.*

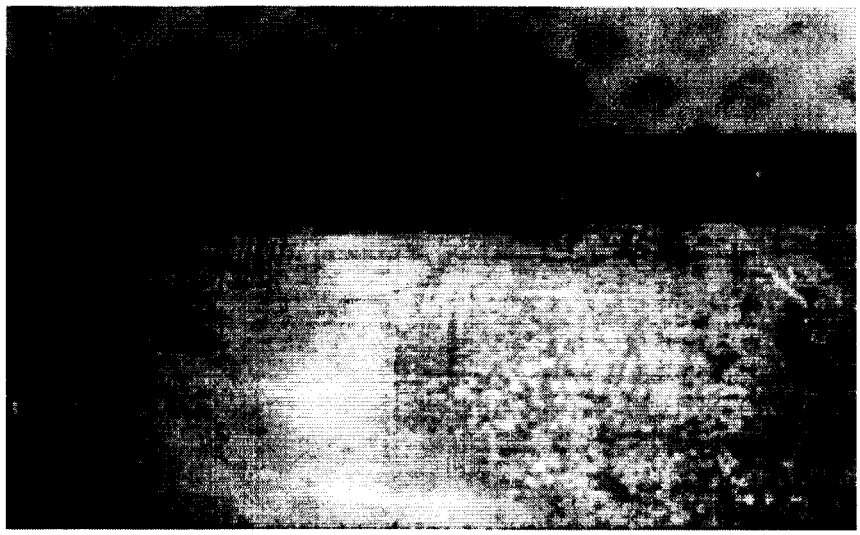

Fig. 17a: Be tiles viewed from the side after the test. We see an undercut between heat sink and tile on three of the four tiles shown. There is also a fault line in the beryllium over several tiles running above the braze. The melt layer depth is estimated at 0.6 mm.

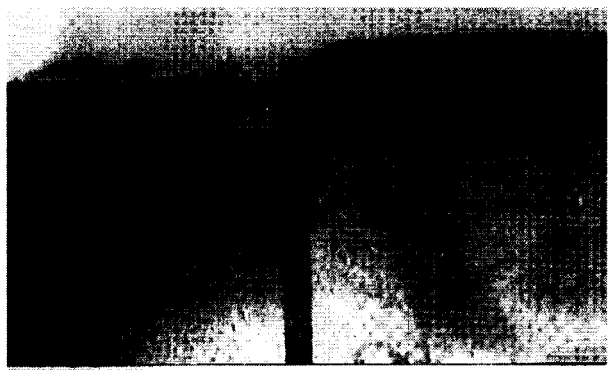

Fig. 17b: Blow up of two tile edges showing the surface damage. Some Beryllium has disappeared at the edge.

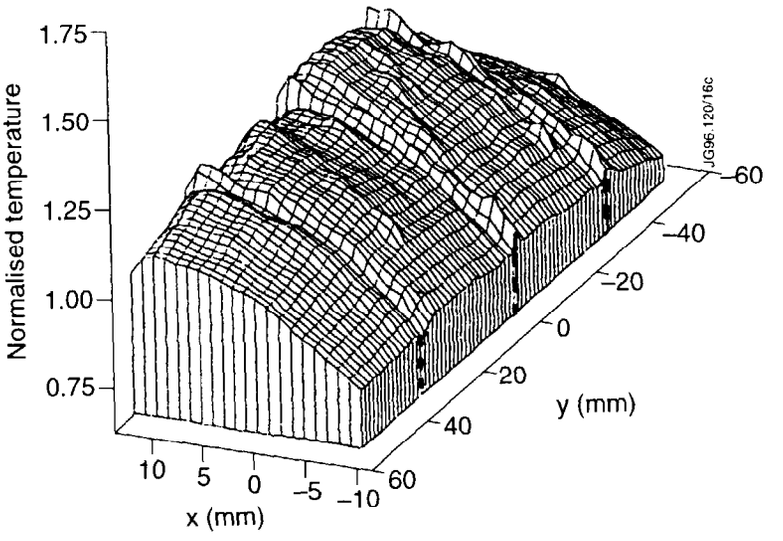

a) before exposure with melting – uniform temperature.

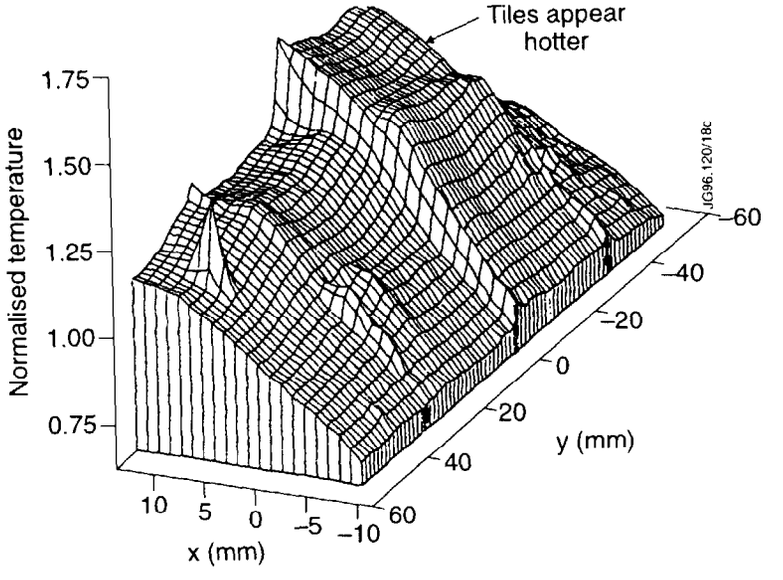

b) after first sequence with surface melting.

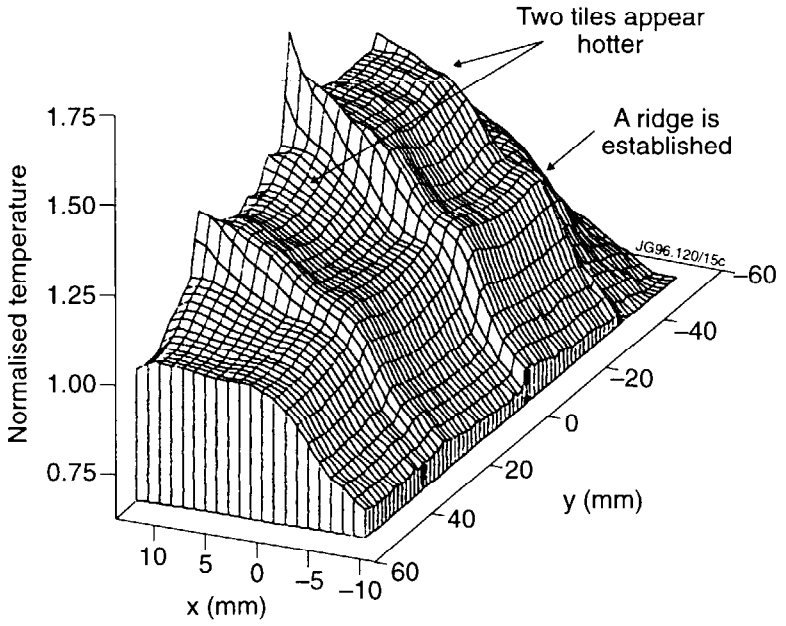

c) after second temperature with surface melting.

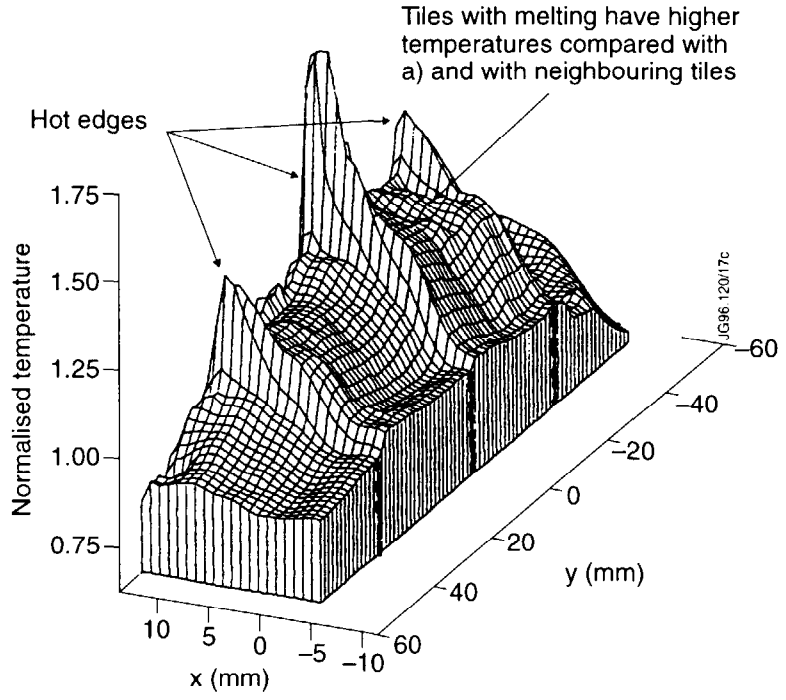

d) after third sequence with surface melting.

Fig. 18: Surface temperature contours before melting and after each melt sequence. The measurements are from unmodulated reference pulses with at least 5 s exposure at approximately 5 MW/m^2. After the first melt sequence the area which is grey in Fig. 12a is hotter (second plot from left). After the second melt series both tiles in the middle are hotter and there is a band with increased gradients between the 400 and 500 degree line. This corresponds to the grey band in Fig. 12b. At the end of the test we see hot spots due to surface damage. The temperature is up by approximately 10 - 20% in these hot spots.

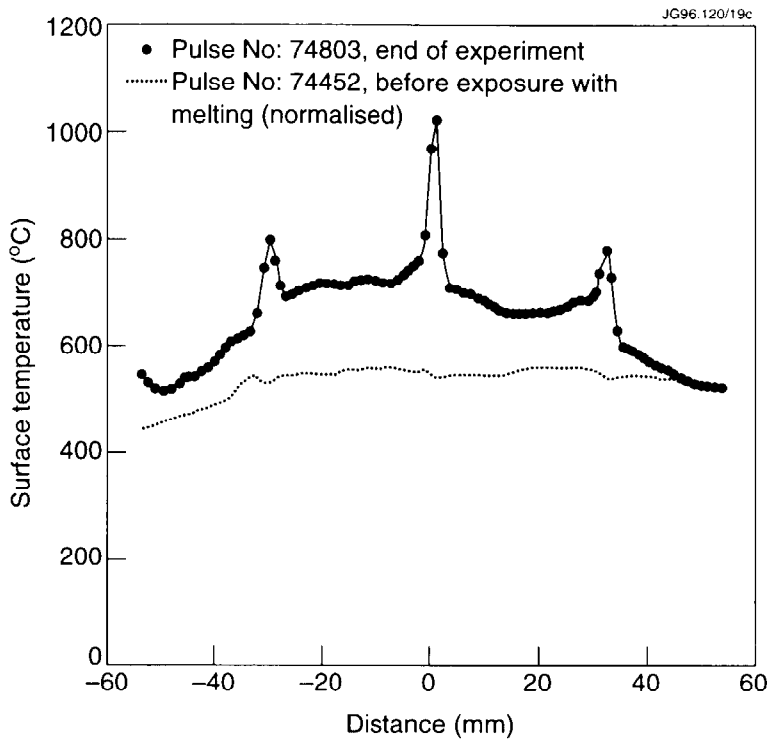

Fig. 19: Change in surface temperature distribution with exposure. The tiles in the centre are hotter (100 - 200 degrees) and show hot spots at the end of the experiment. Early in the experiment the temperature distribution was flat.

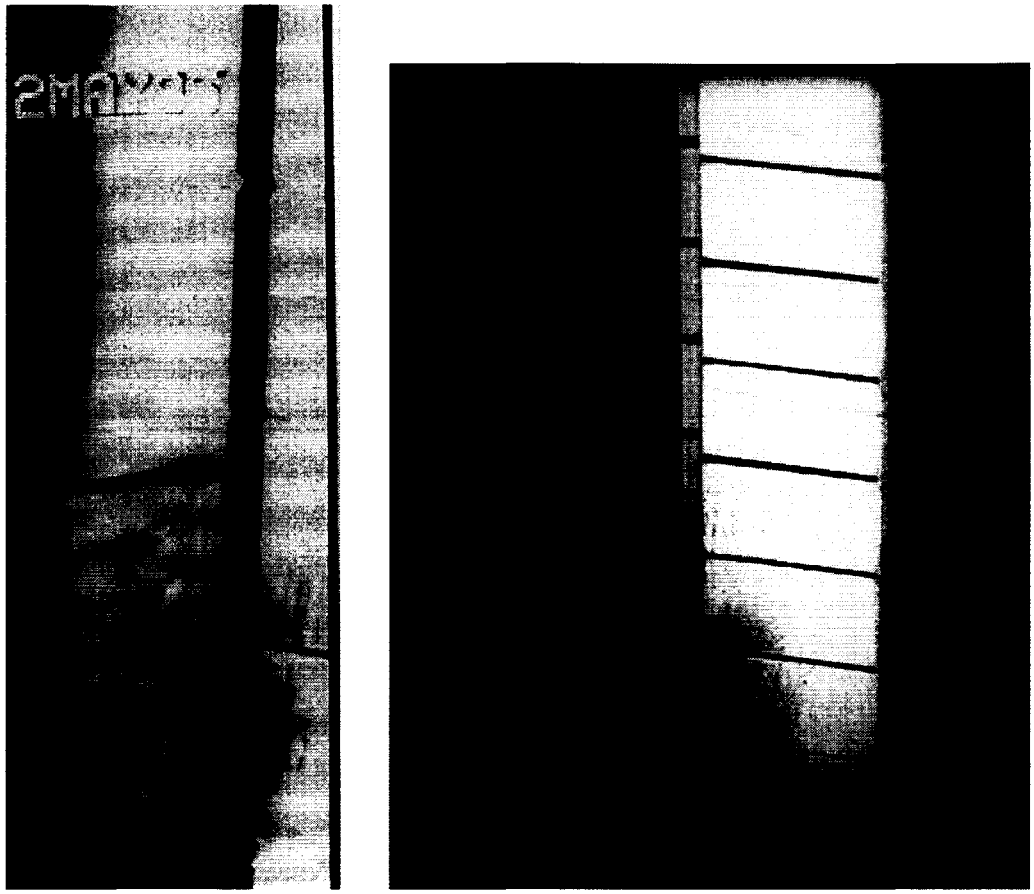

Fig. 20: View on the tile inside the test rig after the second exposure sequence with melting. Left: S-VHS camera with a cold light source. The resolidified Beryllium has a high reflectivity. Right:: Photographic picture of the same object in the same location. The two side scrapers, made from copper appear black as they are completely covered by Beryllium.

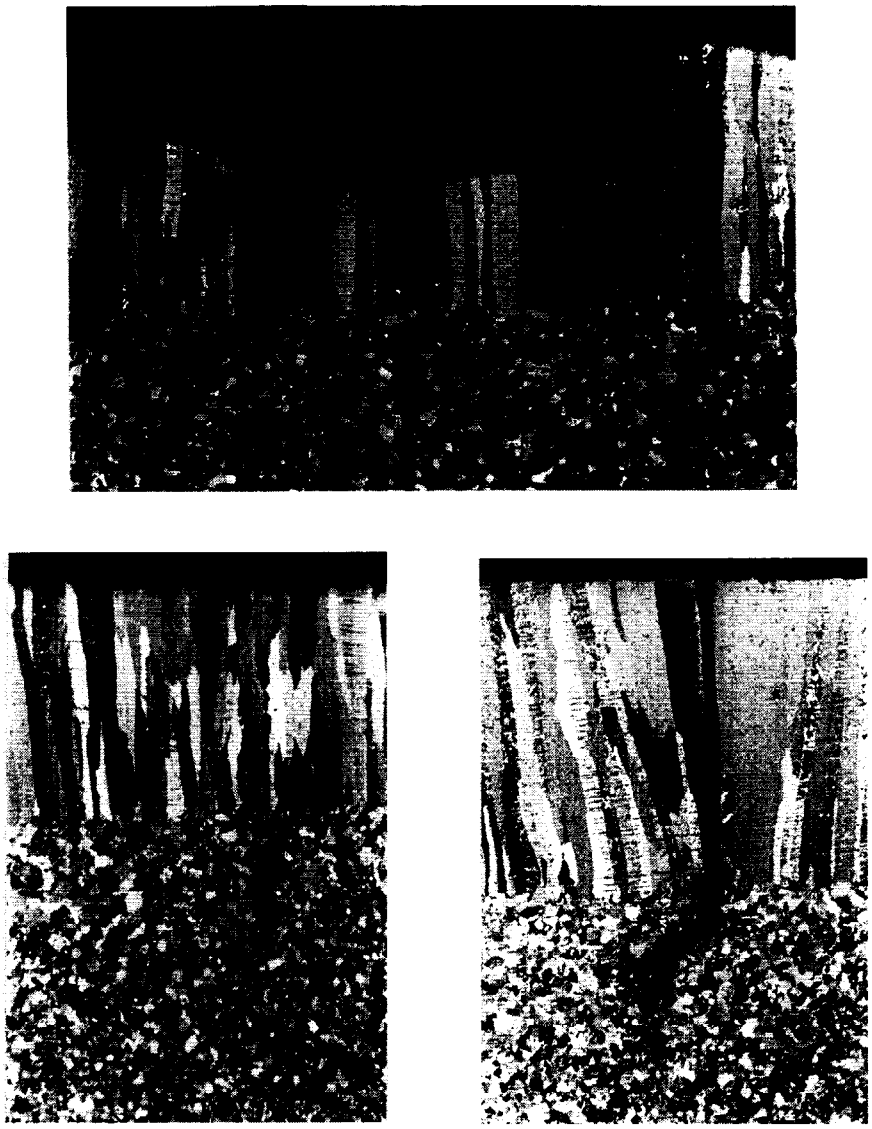

Fig. 21: Micrographs of the hottest tile after the test. The melt layer is up to 0.7 mm deep. Cracks partially penetrate through the melt layer into the base material. Occasionally some of the molten material has flown away.

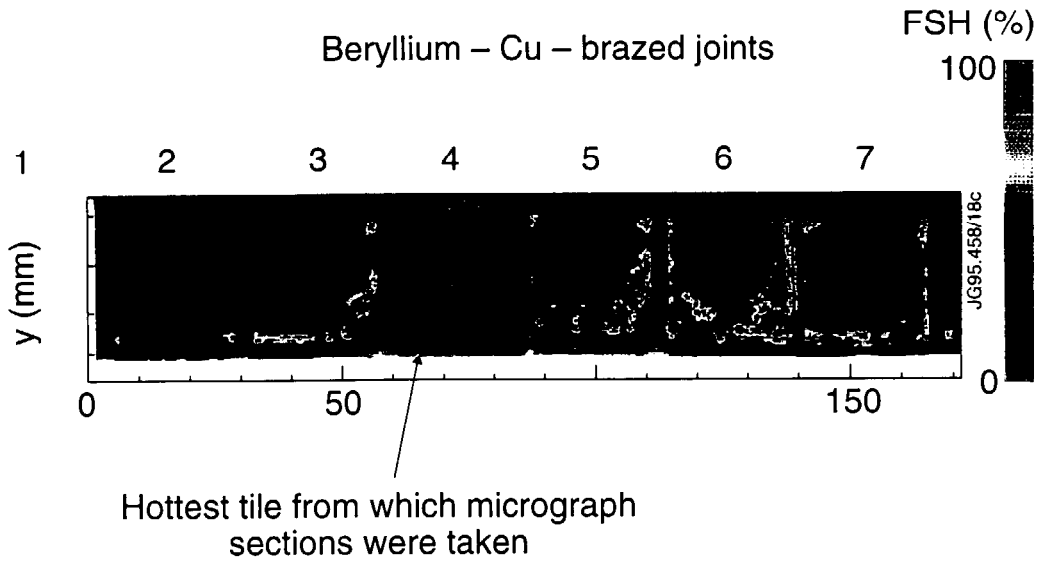

Fig. 22: Ultrasonic test result after the test. The centre of the tiles remains solidly attached, the sides have lost contact.

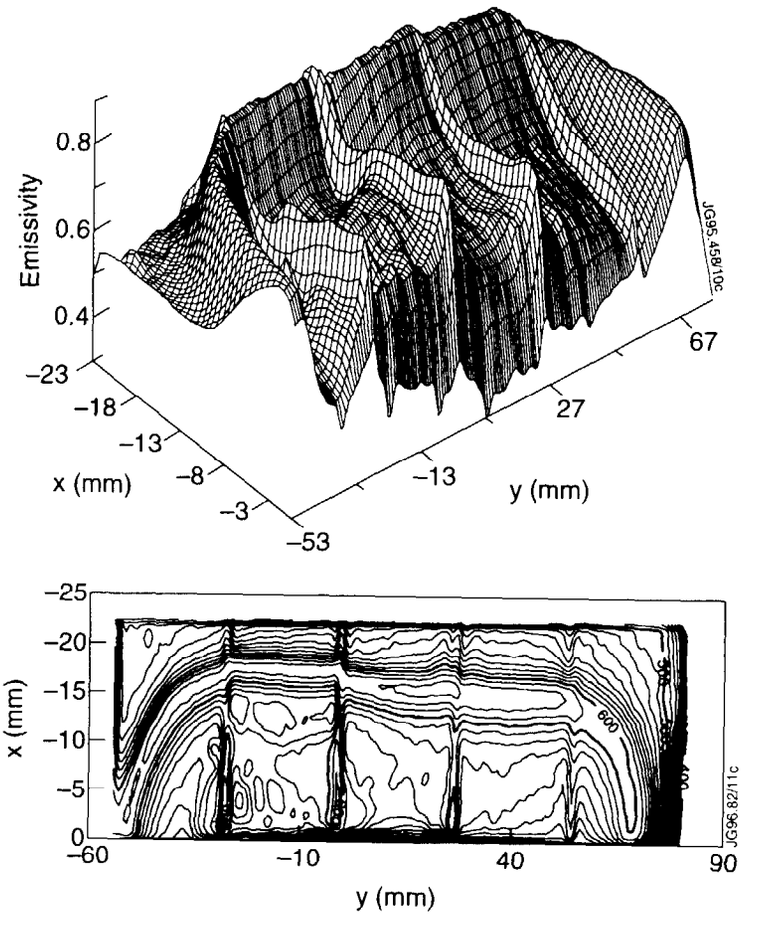

Fig. 23: Measured surface temperature distribution of the test section in thermal equilibrium (470 ^0C) (bottom). To reproduce a constant surface temperature of 470 ^0C we have to use the emissivity distribution shown on the top.

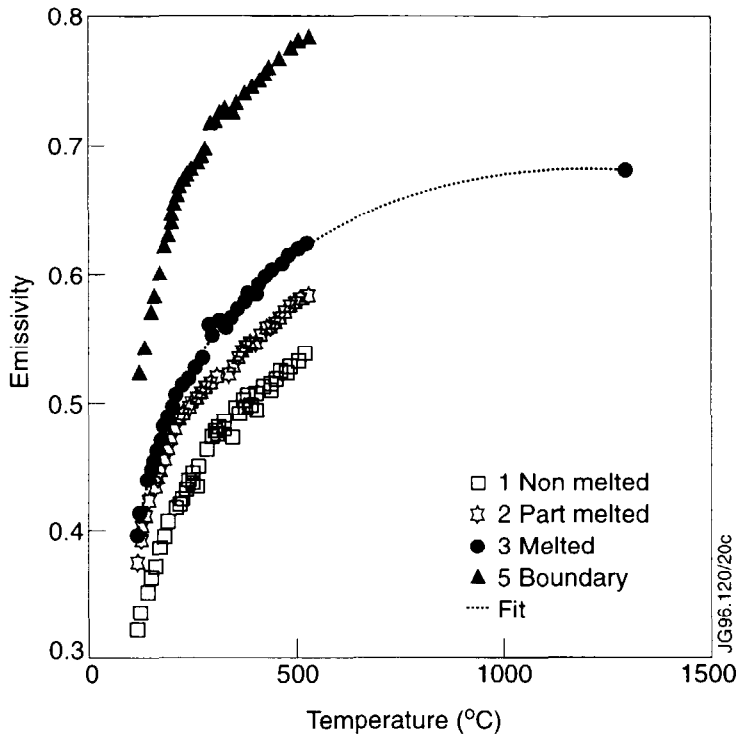

Fig. 24: Emissivity for 4 areas as a function of temperature. In the previously melted area the liquidus temperature can be used as additional calibration point (Fig. 15).

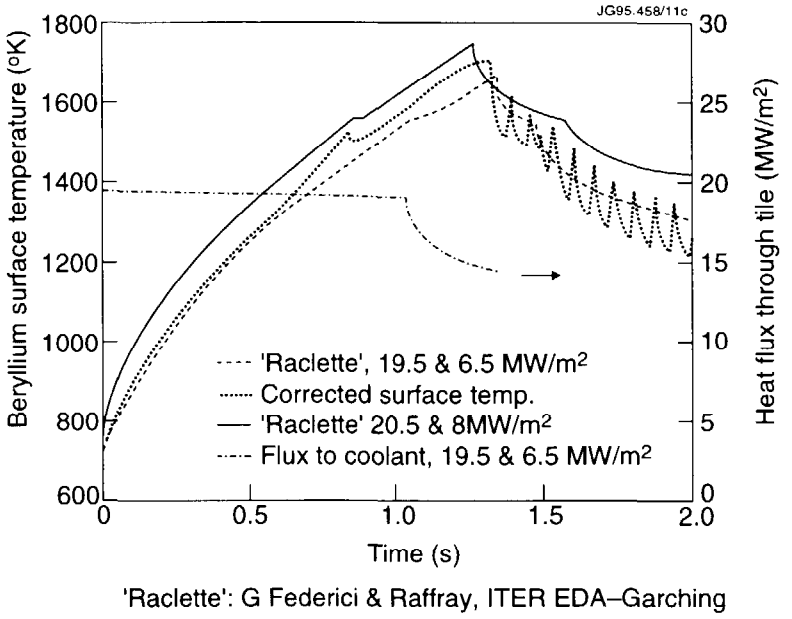

Fig. 25: Output from the ITER model raclette for 15.5 and 20.5 MW/m^2. At 20.5 MW/m^2 the onset of melting coincides but the recondensation phase is longer than observed, at 19.5 MW/m^2 the recondensation phase is as observed but the onset of melting is too late.

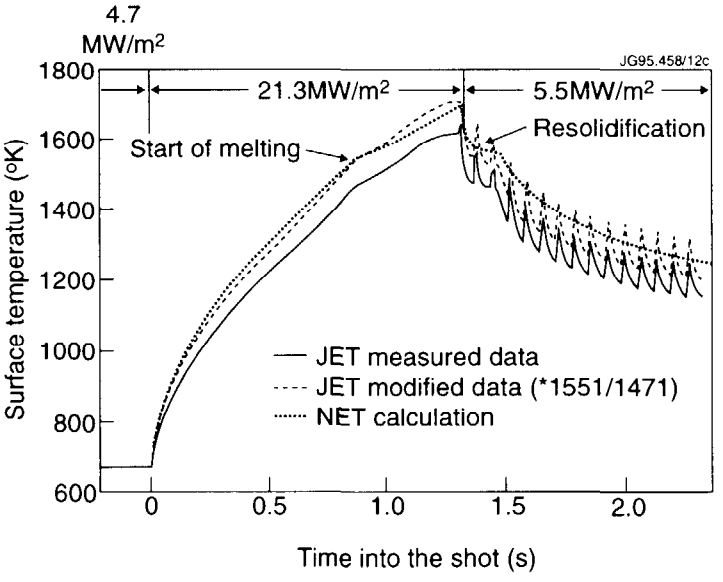

Fig. 26: Output from the NET finite element model. The good agreement is forced by adjusting the power density in the in the modulated exposure after melting. This is justified as the power density is not accurately known during this fast modulation and exposure is also interrupted by breakdowns (Fig. 6).

Annex.1: Unmodulated Pulses

Pulse Number	Notes	Voltage [kV] corrected	G1 Current [A] corrected	Extracted power [MW]	Peak PD [MW/m²]	Peak PD [MW/m²]	Beam On Time [s] set	Beam On Time [s] measured	Cumulative On Time [s]	peak surface temp.
	Be tile (10mm) brazed on vapotron				Water Cal	Inertial Cal				
FORMULAS				**0.00**					**2512.1**	
74384	*Start of Ops – Pulse aborted CISS shutdown*			*0.00*			*2.045*		*2512.1*	
74385	*Start of Ops – Pulse aborted CISS shutdown*			*0.00*			*2.045*		*2512.1*	
74386	*Pulse OK – but not good*	*42.20*	*10.90*				*2.045*	*0.050*	*2512.2*	
74387	*R/A Control Error*	*41.20*		*0.00*			*2.045*	*0.000*	*2512.2*	
74388	*G3 Under Volts*	*43.70*	*2.20*	*0.10*			*2.045*	*0.010*	*2512.2*	
74389	*G3 Error*	*42.90*	*12.86*				*2.045*	*0.010*	*2512.2*	
74390	*G3 Error – reducing gas flow*	*42.90*	*2.18*	*0.09*			*2.045*	*0.090*	*2512.3*	
74391	*Filaments de-selected – Still G3 Error*	*42.90*		*0.00*			*2.045*		*2512.3*	
74392	*G3 under voltage*	*43.00*		*0.00*			*2.045*		*2512.3*	
74393	*No G3 Error*	*43.00*		*0.00*			*2.045*		*2512.3*	
74394	*Re-select filaments – good pulse*	*42.90*	*2.17*	*0.09*			*2.045*	*0.470*	*2512.7*	
74395	*G3 Error*	*42.80*	*2.29*	*0.10*			*2.045*	*0.010*	*2512.7*	
74396		42.90	2.18	0.09			2.045	1.070	2513.8	
74397		42.80	2.18	0.09			2.045	1.330	2515.1	
74398		42.80	2.24	0.10			2.045	1.540	2516.7	
74399	*G3 Error*	*42.70*	*2.32*	*0.10*			*2.045*	*0.420*	*2517.1*	
74400		42.90	2.32	0.10			2.045	1.900	2519.0	
74401		42.80	2.39	0.10	4.16	4.98	2.045	1.520	2520.5	
74402	*Align IR camera*	*42.90*	*2.44*	*0.10*			*2.045*	*0.160*	*2520.7*	
74403		43.00	2.46	0.11			2.045	1.740	2522.4	
74404		43.00	2.40	0.10			5.045	4.270	2526.7	
74405	*G3 under volt*	*43.00*	*2.46*	*0.11*			*5.045*	*0.010*	*2526.7*	
74406		43.00	2.46	0.11			5.045	3.670	2530.4	
74407	*MODULATION ON – G3 U/V*	*42.30*	*2.86*	*0.12*			*5.045*	*0.130*	*2530.5*	
74408		43.10	2.48	0.11			5.045	3.690	2534.2	
74409	*G3 U/V*	*42.90*	*2.61*	*0.11*			*5.045*	*0.210*	*2534.4*	
74410	Modulation off	43.10	2.52	0.11	4.07	4.32	5.045	4.400	2538.8	
74411			2.52	0.00			5.045	5.010	2543.8	
74412	*G3 Error*	*43.20*	*2.59*	*0.11*			*5.045*	*0.340*	*2544.2*	
74413		43.10	2.54	0.11			5.045	4.890	2549.0	
74414		43.10	2.54	0.11			5.045	4.570	2553.6	
74415		43.10	2.55	0.11			5.045	4.840	2558.5	
74416	*G3 Error – Under Volt*	*48.00*	*3.22*	*0.00*			*5.045*	*0.000*	*2558.5*	
74417		48.20	2.98	0.14			3.045	1.540	2560.0	
74418		48.10	2.96	0.14	5.94	4.96	3.045	2.950	2562.9	
74419		48.20	2.87	0.14	5.49	5.05	3.045	3.000	2565.9	
74420		48.20	2.93	0.14			3.045	2.990	2568.9	
74421		48.20	2.96	0.14			3.045	3.030	2572.0	
74422	G3 Error	52.40	3.43	0.18			4.045	1.300	2573.3	
74423	*Tetrode O/V*	*52.20*	*3.36*	*0.18*			*4.045*	*0.970*	*2574.2*	
74424	*G3 Error*	*52.40*	*3.81*	*0.20*			*4.045*	*0.090*	*2574.3*	
74425	*G3 Under Voltage*	*52.30*	*3.68*	*0.19*			*4.045*	*0.020*	*2574.3*	
74426	*G3 Under Voltage*	*53.50*	*5.25*	*0.28*			*4.045*	*0.020*	*2574.4*	

Annex.1: Unmodulated Pulses

Pulse Number	Notes	Voltage [kV] corrected	G1 Current [A] corrected	Extracted power [MW]	Peak PD [MW/m²]	Peak PD [MW/m²]	Beam On Time [s] set	Beam On Time [s] measured	Cumulative On Time [s]	peak surface temp.
	Be tile (10mm) brazed on vapotron				Water Cal	Inertial Cal				
FORMULAS				**0.00**					**2512.1**	
74427	*G3 Under Voltage*			*0.00*			*4.045*	*0.000*	*2574.4*	
74428	*G3 Under Voltage*	*52.50*	*3.55*	*0.19*			*4.045*	*0.060*	*2574.4*	
74429		*52.40*	*3.61*	*0.19*			*4.045*	*0.660*	*2575.1*	
74430	*G3 Under Voltage*	*52.40*	*3.63*	*0.19*			*4.045*	*0.020*	*2575.1*	
74431		52.30	3.47	0.18			4.045	2.990	2578.1	
74432		52.30	3.43	0.18	*7.05*	*6.12*	4.045	3.950	2582.0	
74433	G3 Error	52.20	3.43	0.18			4.045	1.700	2583.7	
74434	G3 Error	52.20	3.42	0.18			4.045	3.130	2586.9	
74435	*G3 Error*			*0.00*			*4.045*	*0.000*	*2586.9*	
74436	*No Arc*			*0.00*			*4.045*		*2586.9*	
74437	*PS Test Pulse*			*0*			*4.045*		*2586.8*	
74438	*PS Test Pulse*			*0*			*4.045*		*2586.8*	
74439	PS Test Pulse	52.2	3.55	0.19			4.045	1.08	2587.9	
74440		52.2	2.96	0.15			4.045	4.03	2591.9	
74441	G3 Under Voltage	52.3	3.05	0.16			4.045	1.89	2593.8	
74442.00	*G3 Under Voltage*	*52.50*	*4.03*	*0.21*			*4.05*	*0.07*	*2593.90*	
74443.00				*0.00*			*4.05*		*2593.90*	
74444		*52.4*	*3.17*				*4.045*	*4.03*	*2597.9*	
74445.00				*0.00*			*4.05*		*2597.90*	
74446.00	*G3 Under Voltage and Tetrode O/V*	*50.70*	*3.11*	*0.16*			*4.05*	*0.47*	*2598.40*	
74447		52.3	3.18	0.17			4.045	4.03	2602.4	
74448		52.4	3.25	0.17	*7.47*	*6.73*	4.045	4.01	2606.4	
74449		52.4	3.24	0.17	*8.53*	*6.83*	4.045	4.03	2610.4	
74450	Increase pulse length to bring Be	52.3	3.28	0.17			4.045	4.01	2614.5	
74451	towards surface melting temperature	52.2	3.33	0.17	*7.02*	*6.98*	5.045	5.02	2619.5	
74452		52.3	3.37	0.18	*7.54*	*6.94*	6.045	6	2625.50	
74453	Increase power density	58.7	3.75	0.22	*7.59*	*7.72*	2.045	2	2627.5	
74454		58.7	3.72	0.22			2.045	2.02	2629.5	
74455		58.6	3.94	0.23	*9.49*	*7.55*	2.045	2.02	2631.5	744
74456.00	*Unit 1 tet O/V*	*54.50*	*3.55*	*0.19*			*3.05*	*0.01*	*2631.50*	
74457		58.7	3.85	0.23	*8.50*	*7.71*	3.045	3	2634.5	906
74458.00	*Unit 2 threshold 2*	*59.00*	*3.82*	*0.23*			*3.55*	*0.02*	*2634.50*	
74459.00	*Unit 1 Crowbar*			*0.00*			*3.55*		*2634.5*	
74460		58.7	3.84	0.23	*7.85*	*7.66*	3.545	3.51	2638.1	945
74461	Unit 1 tet O/V	58.6	3.88	0.23			4.045	1.63	2639.7	
74462.00	*Unit 1 tet O/V – G3 Error U/V*	*58.20*	*4.34*	*0.25*			*4.05*	*0.05*	*2639.70*	
74463		58.7	3.87	0.23	*8.85*	*7.65*	4.045	3.98	2643.7	979
74464		58.6	4.25	0.25	*10.63*	*9.13*	2.045	2	2645.7	899
74465		58.6	4.29	0.25			2.045	2.03	2647.7	
74466		58.6	4.25	0.25	*10.08*	*8.96*	2.545	2.52	2650.3	1007
74467.00	*Unit 2 threshold 2*	*67.30*	*5.07*	*0.34*			*1.05*	*0.04*	*2650.30*	
74468.00		*67.00*	*5.25*	*0.35*			*1.05*	*0.24*	*2650.50*	
74469		68.4	5.01	0.34			1.045	0.63	2651.2	

Annex.1: Unmodulated Pulses

Pulse Number	Notes	Voltage [kV] corrected	G1 Current [A] corrected	Extracted power [MW]	Peak PD [MW/m²]	Peak PD [MW/m²]	Beam On Time [s] set	Beam On Time [s] measured	Cumulative On Time [s]	peak surface temp.
	Be tile (10mm) brazed on vapotron									
					Water Cal	Inertial Cal				
FORMULAS				**0.00**					**2512.1**	
74470		68.7	5.17	0.36	*13.46*	*13.40*	1.045	0.91	2652.1	
74471		68.5	5.38	0.37	*15.11*	*13.54*	1.045	1	2653.1	986
74472	Modulation ON	68.6	5.14	0.35	*12.21*	*13.21*	1.045	0.68	2653.8	660
74473		68.7	5.23	0.36	*12.10*	*12.31*	2.045	1.32	2655.1	860
74474		**68.5**	**5.25**	**0.36**	*13.18*	*12.60*	**3.045**	**1.97**	**2657.1**	**1018**
74475	IR Camera Line Scan	68.6	5.17	0.35	*10.68*	*11.75*	3.045	2.04	2659.1	

Annex.2: Pulses with beam modulation

Pulse Number	Notes	Voltage [kV] corrected	G1 Current [A] corrected	Extracted power [MW]	Peak PD [MW/m²]	Peak PD [MW/m²]	On-time measured	Cumulative On Time [s]	Max Braze Temp [°C]
	Be tile (10mm) brazed on vapotron								
					Water Cal	Inertial Cal			
FORMULAS				**0.00**				**2512.1**	
74476	*PSU Test Pulse*		*3*	*0.00*			*1.5*	*1.50*	
74477	*PSU Test Pulse*		*3.4*	*0.00*			*3*	*4.50*	
74478	*PSU Test Pulse*		*3.32*	*0.00*			*3.02*	*7.52*	
74479	*PSU Test Pulse*		*3.91*	*0.00*			*0.12*	*7.64*	
74480	*PSU Test Pulse*			*0.00*				*7.64*	
74481	*PSU Test Pulse*			*0.00*				*7.64*	
74482	*PSU Test Pulse*		*3.41*	*0.00*			*2.98*	*10.62*	
74483	*PSU Test Pulse*		*3.66*	*0.00*			*3*	*13.62*	
74484	*PSU Test Pulse*		*3.75*	*0.00*			*2.96*	*16.58*	
74485	*PSU Test Pulse*		*3.7*	*0.00*			*3.02*	*19.60*	
74486	*PSU Test Pulse*		*3.79*	*0.00*			*3.02*	*22.62*	
74487	*PSU Test Pulse*		*3.84*	*0.00*			*3.02*	*25.64*	
74488	Start of Ops with new modulation system	42.80	2.21	0.09			3.640	*29.28*	
74489	No beam modulation when requested	42.80	2.21	0.09			3.960	*33.24*	
74490	No beam modulation when requested	42.90	2.22	0.10	*5.53*	*4.26*	3.990	*37.23*	
74491	*Modulation ON – Wrong Mark/Space*	*42.695*	*2.27*	*0.10*			*0.7*	*37.93*	
74492	Modulation ON – Only first window	42.80	2.19	0.09			1.530	*39.46*	
74493	Modulation OK – 3 windows tested	42.90	2.18	0.09			2.400	*41.86*	
74494	*Setup for 20 MW/m²*	*67.795*	*5.23*	*0.35*			*0.41*	*42.27*	
74495		*68.295*	*5.39*	*0.37*	*12.80*	*12.41*	*0.76*	*43.03*	
74496		*71.695*	*4.58*	*0.33*	*16.15*	*15.82*	*0.72*	*43.75*	
74497		*71.695*	*4.68*	*0.34*	*16.00*	*15.50*	*0.81*	*44.56*	
74498		*71.895*	*4.82*	*0.35*	*16.64*	*16.18*	*0.77*	*45.33*	
74499	*Modulation ON*	*71.195*	*5.4*	*0.38*			*0.17*	*45.50*	
74500	Set 20 msec on 60 msec off & 200 msec	71.40	5.09	0.36	*19.89*	*16.19*	1.060	*46.56*	
74501	300 msec on at the end	71.40	5.11	0.36	*21.42*	*16.89*	1.260	*47.82*	
74502	400 msec on at the end	71.10	5.17	0.37			1.250	*49.07*	
74503		71.50	5.33	0.38	*18.85*	*17.82*	1.330	*50.40*	
74504		71.80	5.46	0.39	*19.87*	*18.00*	1.280	*51.68*	
74505		71.80	5.56	0.40	*22.40*	*18.73*	1.350	*53.03*	
74506	480 msec on at the end	71.10	5.64	0.40	*20.72*	*19.21*	1.350	*54.38*	
74507	20 msec on 60 msec off continuous	71.30	5.77	0.41	*21.86*	*18.98*	1.500	*55.88*	
74508		71.20	5.93	0.42			1.380	*57.26*	
74509	Delay of 20ms between windows	71.70	6.15	0.44			1.250	*58.51*	
74510	600 msec on at the end	71.70	6.24	0.45			1.450	*59.96*	

Annex.2: Pulses with beam modulation

Pulse Number	Notes	Voltage [kV] corrected	G1 Current [A] corrected	Extracted power [MW]	Peak PD [MW/m²]	Peak PD [MW/m²]	On-time measured	Cumulative On Time [s]	Max Braze Temp [°C]
	Be tile (10mm) brazed on vapotron								
					Water Cal	**Inertial Cal**			
FORMULAS				**0.00**				**2512.1**	
74511	20/60 on/off 700 on 30/60 on/off	71.50	6.38	0.46	*24.23*	*20.67*	1.780	*61.74*	
74512		71.60	6.44	0.46	*23.63*	*21.24*	1.920	*63.66*	
74513	20/60 on/off 800 on 30/60 on/off	71.50	6.52	0.47	*22.73*	*21.53*	1.930	*65.59*	
74514		71.50	6.59	0.47	*22.63*	*21.52*	2.000	*67.59*	
74515	20/60 on/off 800 on 35/60 on/off	71.70	6.62	0.47	*22.94*	*22.15*	2.050	*69.64*	
74516	Aborted PS deselected			0.00				*69.64*	
74517	20/60 on/off 1000 on 35/60 on/off	71.40	6.25	0.45	*21.86*	*19.48*	2.510	*72.15*	
74518		71.70	6.35	0.46	*20.04*	*19.07*	2.480	*74.63*	
74519	MOD ON 20 msec on 60 msec off Gas d'bled			0.00			1	*75.63*	
74520		67.69	5.16	0.35	*16.65*	*15.55*	1.44	*77.07*	
74521		67.89	5.45	0.37	*17.68*	*16.53*	1.58	*78.65*	
74522		67.49	5.54	0.37	*18.48*	*16.77*	1.58	*80.23*	
74523		67.39	5.52	0.37	*20.13*	*16.88*	1.57	*81.80*	
74524		67.19	5.64	0.38	*17.42*	*16.95*	1.58	*83.38*	
74525	4 sec of 20/60 & 1 sec on & 2 sec 14/20	67.69	5.73	0.39	*18.76*	*18.12*	2.55	*85.93*	
	01 - May - 95							*85.93*	
74771							0.00	*85.93*	
74772							0.870	*86.80*	
74773							2.500	*89.30*	
74774							3.000	*92.30*	
	02 - May - 95							*92.30*	
74775					*3.34*	*4.15*	5.000	*97.30*	
74776	G3 U/V TET O/V						0.640	*97.94*	
74777					*3.91*	*4.98*	4.530	*102.47*	
74778					*3.82*	*5.05*	4.510	*106.98*	
74779					*3.54*	*4.98*	4.700	*111.68*	
74780					*15.23*	*20.36*	1.380	*113.06*	
74781					*14.62*	*19.80*	1.150	*114.21*	
74782					*16.07*	*20.79*	1.980	*116.19*	
74783	,800mS ON in middle of beam				*16.71*	*20.81*	2.120	*118.31*	
74784					*16.83*	*21.14*	2.120	*120.43*	
74785	Reapp to 20 mS				*17.43*	*21.03*	2.220	*122.65*	
74786					*17.79*	*21.09*	2.370	*125.02*	
74787					*17.73*	*21.40*	2.350	*127.37*	
74788					*17.72*	*21.43*	2.370	*129.74*	

Annex.2: Pulses with beam modulation

Pulse Number	Notes	Voltage [kV] corrected	G1 Current [A] corrected	Extracted power [MW]	Peak PD [MW/m²]	Peak PD [MW/m²]	On-time measured	Cumulative On Time [s]	Max Braze Temp [°C]
	Be tile (10mm) brazed on vapotron								
					Water Cal	**Inertial Cal**			
FORMULAS				**0.00**				**2512.1**	
74789	***,1.1 Sec ON***				*15.72*	*20.31*	***2.570***	*132.31*	
74790					*17.78*	*20.16*	***2.540***	*134.85*	
74791	***,1.3 Sec ON***				*16.32*	*20.46*	***2.640***	*137.49*	
74792					*15.68*	*20.65*	***2.660***	*140.15*	
	03-May-95							*140.15*	
74793					*3.71*	*5.05*	4.880	*145.03*	
74794					*4.61*	*5.10*	***4.980***	*150.01*	
74795					*14.89*	*16.94*	1.620	*151.63*	
74796	pulse aborted current not changed							*151.63*	
74797					*14.29*	*18.03*	1.590	*153.22*	
74798	**1.5 sec on–usual modulation**				*15.94*	*19.96*	2.590	*155.81*	
74799					*16.19*	*20.11*	2.900	*158.71*	
74800					*16.70*	*20.01*	***2.940***	*161.65*	
74801					*16.68*	*20.36*	***2.950***	*164.60*	
74802	***Back to 5MW/m² – reference shot, sear***				*3.64*	*5.29*	***4.990***	*169.59*	
74803					*4.01*	*5.30*	5.000	*174.59*	